On the Role of Inertial Instability in Stratosphere Troposphere Exchange

Near Midlatitude Cyclones

Shellie M. Rowe and Matthew H. Hitchman

Department of Atmospheric and Oceanic Sciences

University of Wisconsin-Madison, Madison, Wisconsin

Revised submission to *J. Atmos. Sci.*, January 23, 2015

Corresponding Author

Matthew H. Hitchman
Department of Atmospheric and Oceanic Sciences
1225 W. Dayton Street
University of Wisconsin – Madison
Madison, WI 53706
matt@aos.wisc.edu

Abstract. In simulations of midlatitude cyclones with the University of Wisconsin Nonhydrostatic Modeling System (UWNMS), mesoscale regions with large negative absolute vorticity commonly occur in the upper troposphere and lower stratosphere (UTLS), overlying thin layers of air with stratospheric values of ozone and potential vorticity (PV). These locally enhanced stratosphere – troposphere exchange (STE) events are related to upstream convection by tracing negative equivalent potential vorticity (EPV) anomalies along back trajectories. The mutual coincidence of negative absolute vorticity, PV, and EPV, indicating inertial instability in the UTLS, is shown to occur in association with enhanced STE signatures. Here results are presented for two midlatitude cyclones in the upper Midwest where convection develops between the subpolar and subtropical jets.

Mesoscale regions of negative EPV air originate upstream in the boundary layer. As they are transported through convection, EPV becomes increasingly negative toward the tropopause. In association with the arrival of each large negative EPV anomaly, a locally-enhanced poleward surge of the subpolar jet occurs, characterized by high turbulent kinetic energy and low Richardson number. Isosurfaces of wind speed show that gravity waves emanating from inertially unstable regions modulate both jets simultaneously. It is shown that inertially unstable convective outflow surges can facilitate STE locally by fostering poleward acceleration in the UTLS, turbulent entrainment, and enhanced folding of tropospheric air over stratospheric air underneath the subpolar jet.

1. Introduction

a. Motivation

Stratosphere – troposphere exchange (STE) of air in the upper troposphere and lower stratosphere (UTLS) is an essential part of the Brewer-Dobson circulation, which circulates mass between the stratosphere and troposphere, and therefore exerts a primary influence on the distribution of climatically important constituents such as ozone, water vapor, and volcanic aerosol. An abrupt increase in static stability occurs at the tropopause, caused by stratospheric ozone heating, together with surface heating and buoyant adjustment by convection and baroclinic waves in the troposphere (e.g., Manabe and Wetherald, 1967). The extratropical tropopause is defined to occur when the lapse rate is less than 2 K/km, but is often defined by values of Ertel's potential vorticity ($PV = \frac{1}{\rho}\frac{\partial\theta}{\partial z}(f + \zeta)$, where ρ is density, θ is potential temperature, f is the Coriolis parameter, and ζ is relative vorticity) in the range ~ 1 - 4 PVU (1 x 10^{-6} m^2 K kg^{-1} s^{-1}), or of ozone mixing ratio in the range 100-200 ppbv. According to the non-transport theorem (Andrews et al., 1987), diabatic and frictional processes are required for molecules to cross the tropopause (cf. Haynes et al., 1990). STE occurs in the vicinity of thunderstorm tops, breaking Rossby waves, and breaking gravity waves, which cause mixing in the UTLS (Holton et al., 1995). Estimates of STE vary by more than a factor of 2 (e.g., Stohl et al., 2003), highlighting the need for improved understanding of the underlying dynamics.

The present work is motivated by our diagnosis of enhanced STE in conjunction with regions of inertial instability in simulations of many different midlatitude cyclones with the University of Wisconsin Nonhydrostatic Modeling System (UWNMS). These simulations were carried out to investigate wintertime quasi-stationary precipitation features and to better understand the origin of the thin sheets (~hundreds of meters thick) of stratospheric air, which appear to curl poleward and downward into the troposphere near midlatitude jets in association with midlatitude Rossby wave breaking (RWB) (e.g., Danielson, 1968). High resolution dropwinsonde data sampling a wide variety of geographical locations and jet configurations, including cutoff lows (Fig. 4, Shapiro, 1974), southeastward jets (Fig. 5, Shapiro, 1978; Fig. 3, Shapiro, 1980), a digging trough (Fig. 1, Shapiro, 1981), an Icelandic low (Fig. 4, Shapiro, 1985) and a staircase of westerly jets (Fig. 16, Shapiro et al., 1987), illustrate the ubiquitous sharpness and typical structure of stratospheric intrusions. Aircraft campaigns, satellite data analysis, and model analysis of trace constituents have shown that these sheets of air tend to be turbulent and exhibit a mixed stratospheric / tropospheric chemical signal (e.g., Browell et al., 1989; Zahn et al., 2000; Hoor et al., 2002; Stohl et al., 2003; Bowman et al., 2007; Pan et al., 2007; Hegglin et al., 2008). The mystery of how thin stratospheric intrusions are formed strongly motivates the present work.

In examining simulations of quasi-stationary, banded precipitation events in the upper Midwest with the UWNMS, regions of negative equivalent potential vorticity (EPV) were found near the tropopause on the anticyclonic shear side of the jet in the model. As will be demonstrated, negative EPV in the UTLS (where it is statically stable and very dry) implies inertial instability. Adjacent to these negative EPV regions were found layers of turbulently mixed air associated with folds in PV and ozone. In this paper we explore the hypothesis that mesoscale regions of inertial instability near the jet can facilitate STE. The proposed mechanism for STE is that inertial instability causes poleward acceleration of uppermost tropospheric air, leading to a locally enhanced fold, with increased turbulent entrainment of stratospheric air.

b. RWB, inertial instability, and westerly jets

The subtropical westerly jets, which result from a buoyancy-driven redistribution of angular momentum by local Hadley circulations, are collocated with strong baroclinic energy conversion processes, as synoptic scale Rossby waves amplify, break, and are absorbed in the UTLS (Andrews et al., 1987). Often a subpolar jet near 300 hPa (315-330 K) is present simultaneously with a subtropical westerly jet near 200 hPa (340-350 K) (e.g., Christenson and Martin, 2014). RWB occurs in 3D, with occlusion leading to a reversal of the normally positive meridional gradient of PV, and tropopause folds. RWB implies a cascade of energy to smaller scales, with small-scale mixing and radiative damping required for wave absorption (e.g., McIntyre and Palmer, 1983). Convective, Kelvin-Helmholtz, inertial, and baroclinic instabilities tend to generate gravity waves. Gravity waves also amplify, break, and are absorbed through small-scale mixing and radiative damping. Turbulence from breaking waves and instability is required for STE.

A discussion of cyclonic and anticyclonic RWB, together with transport pathways in midlatitude cyclones, is given by Thorncroft et al. (1993). The warm conveyor belt (WCB) can split, with one branch curving cyclonically poleward, often riding up and over part of the lower stratosphere, and plays a central role in the present work. This can contribute to the identification of multiple tropopauses (e.g., Randel et al., 2007). The dry stratospheric conveyor belt (DCB), which typically curves cyclonically equatorward into the troposphere, may aid the formation of stratospheric intrusions by differential advection. Stratospheric intrusions often take the form of elongated PV streamers as seen at constant height and thin sheets as seen in cross-sections. These dry intrusions are sometimes related to severe wind events at the surface (Browning and Reynolds, 1994) and forest fire outbreaks (Zimet et al., 2007; Schoeffler, 2013).

In quasi-geostrophic theory, a preferred region of poleward and downward circulation is expected to occur near the jet entrance region (e.g., Markowski and Richardson, 2010). Cold air advection along the UTLS jet axis promotes a preference for sinking downstream of a trough at synoptic scales, via the Sutcliffe development mechanism (Martin, 2006; Lang and Martin, 2010). Sawyer (1949) explored the possible role of inertial or symmetric instability in the UTLS in modifying midlatitude cyclogenesis, jet stream behavior, and meridional circulations. It is now understood that inertial instability plays a role in establishing quasi-stationary precipitation bands in midlatitude cyclones (e.g., Bennetts and Hoskins 1979; Knox 2003), and phenomena on the edges of anticyclones (Stevens and Ciesielski 1986; Knox 1997). Jones and Thorpe (1992) studied 3D inertial instabilities resulting from a region of negative PV and concluded that the phenomenon is fundamentally the same as classical 2D symmetric instability.

Sato and Dunkerton (2002) showed that conditions are inertially unstable more than 20% of the time in the upper troposphere on the equatorward side of the subtropical westerly jet south of Japan during boreal winter. They found that the existence of distinctive layered perturbations in the UTLS corresponded with times of inertial instability. Schumacher and Schultz (2000) also found that inertially unstable conditions are common in the subtropical troposphere. Knox and Harvey (2005) compiled a climatology of inertial instability and RWB and found that it is inertially unstable over 2-5% of the midlatitude UTLS at any given time.

Planetary Rossby waves refracting into the tropical middle atmosphere encounter inertially instable conditions, thereby exciting quasi-stationary 3D circulations, with vertical motions leading to “pancake structures” in the temperature field (Hitchman et al. 1987; Hayashi et al., 2002). As RWB proceeds, air with anomalous PV is advected across the equator, with resultant inertial instability and overturning circulations. The associated divergence /

convergence fields ensure that the horizontal and vertical scales of inertial instability are smaller than Rossby waves, facilitating an enstrophy cascade during RWB and helping to homogenize PV (O'Sullivan and Hitchman, 1992).

c. Convective influences on STE near jets

A growing body of literature explores the role of latent heating variations during ascent in the WCB in creating mid-tropospheric positive PV anomalies and upper tropospheric negative PV anomalies (Pomroy and Thorpe, 2000; Knippertz and Wernli, 2010; Lang, 2011; Schemm et al., 2013; Madonna et al., 2013). These papers guide our interpretation of heating along trajectories through convection embedded within the WCB.

Cooper et al. (2004) showed that penetration of stratospheric intrusions by convection facilitates subsequent mixing into the troposphere. Homeyer et al. (2011) found that convection into stratospheric intrusions can yield a distinctive mixture of more than 125 ppmv H_2O and 100 ppbv O_3. Griffiths et al. (2000) argued that the PV anomaly associated with a fold can help to induce convection. Conversely, Lang (2011) showed that convection can lead to intensification of lower stratospheric fronts.

An example of ozone STE associated with a convective complex over China in March 2001 is described by Hitchman et al. (2004) and Kittaka et al. (2004), where STE occurred via self-induced peripheral descent, similar to the circulation around an atomic explosion or idealized warm bubble simulation (e.g., Fig. 5, Wicker and Skamarock, 1998). The convective complex occurred in the westerly jet south of Japan, and thereby had access to high ozone in the UTLS on the poleward side of the jet. Aircraft and UWNMS diagnoses showed that air with high PV, high ozone, and very low water vapor curled downward and inward to ~6.5 km and promoted the decay phase of the complex. It will be shown that, in the cases studied here, enhanced stratospheric intrusions immediately follow convective injection of negative PV, inertially unstable air at jet level.

Hoggatt and Knox (1998) studied an elevated convection event in the upper Midwest during 14 July 1995 and discovered that elongated bands of light rain tend to coincide with a narrow region of negative PV. Simulations of the event indicated a quadrupole checkerboard pattern in the vertical motion field, signifying inertial instability, as in the equatorial middle atmosphere. Schumacher et al. (2010) simulated quasi-stationary precipitation bands and found that they occurred in an environment with a well-mixed baroclinic boundary layer, positive convective available potential energy, and widespread negative PV. They argued that ascent caused by frontogenesis and banded moist convection produced narrow regions of negative absolute vorticity directly by the upward transport of low-momentum air. Convective bands initiated within the ascending branch of the secondary circulation were associated with elevated and near-surface frontogenesis. Their work is explicit about the presence of negative PV, and inertial instability on the poleward side of the surface cyclone and anticyclonic side of the jet. Their focus, however, was on the cause of the precipitation maximum and to compare simulated versus observed convective bands near complex terrain.

d. Organization of paper

Dynamical diagnostic quantities are introduced in section 2, while the data and simulations are described in section 3. In sections 4 and 5 two case studies with the UWNMS are presented which feature pronounced, quasi-stationary, elongated precipitation bands common in the upper Midwest during winter and spring. The 3D relationship among the locations of the jets, negative EPV, meridional flow, upstream convection, and synoptic storm features is highlighted. The intimate temporal linkage between negative EPV anomalies, the signature of sharpened stratospheric intrusions, and gravity waves connecting the jets is shown in supplementary film loops. Case 2 features the signature of STE as seen in ozone initialized in the UWNMS with globally assimilated ozone from the Goddard Earth Observing System (GEOS ozone) (Stajner et al., 2008). A summary statement of the proposed mechanism, together with a schematic diagram, are given in section 6. It will be argued that inertial instability facilitates STE by causing "overfolds" in the UTLS, as part of the baroclinic energy conversion process arising from air masses of different density subject to gravity and rotation.

2. Dynamical diagnostics

a. Inertial instability, absolute vorticity, and PV

This section relates inertial instability to negative EPV and introduces the PV tendency equation. Inertial instability occurs when angular momentum decreases radially outward, such as in flow between two rotating cylinders (Rayleigh, 1916; Taylor, 1923). When this criterion for instability is met, parcels accelerate and rearrange themselves, tending to stabilize the angular momentum profile. Conversely, one might expect resistance to radial motion when angular momentum increases with radius. Knox (2003) provides a clear interpretation and comprehensive overview of inertial instability theory and related phenomena.

Consideration of radial parcel displacement δs in an axisymmetric vortex yields the oscillator equation

$$\frac{\partial^2}{\partial t^2}\delta s = - f\,(f + \zeta)\,\delta s\,, \tag{1a}$$

with acceleration occurring (inertial instability) if the coefficient is negative:

$$f\ (f + \zeta) < 0\ , \qquad (1b)$$

where $f = 2\ \Omega \sin\varphi$ and $\zeta = \partial v/\partial x - \partial u/\partial y$ is relative vorticity (Eliassen and Kleinschmidt, 1957; Holton, 2006). From the reference from of the earth's rotation axis, absolute angular momentum per unit mass is given by $m = r\,u + r^2\,\Omega$, where $r = a \cos\varphi$, a is earth radius, u is zonal flow, and Ω is the angular frequency of the earth's rotation. Inviscid inertial instability will occur in sufficiently strong anticyclonic relative vorticity, which can occur on the equatorward flank of a westerly jet. Inertial instability implies a divergence / convergence pattern associated with parcel acceleration and deceleration at the edges of inertially unstable regions, which in turn implies 3D circulations, enhanced turbulence, and mixing (O'Sullivan and Hitchman, 1992).

The inertial instability criterion is related to Ertel's potential vorticity (PV) and the gradient of angular momentum on an isentropic surface as follows:

$$f\ PV = \frac{1}{\rho}\frac{\partial\theta}{\partial z}\,f\,(f + \zeta) = -\,\frac{1}{r}\,\nabla_\theta\, m\ <\ 0 \quad , \qquad (2)$$

(e.g., Hoskins et al., 1985; Hitchman and Leovy, 1986). Inertial instability occurs when there is anomalously-signed PV for a given hemisphere, or anomalous absolute vorticity (first relation in (2)). It occurs when angular momentum increases toward the rotation axis (second relation in (2)). This criterion for instability is easier to satisfy near the equator where f is small and angular momentum surfaces are parallel to the surface of the earth. In the Northern Hemisphere, where $f > 0$, the flow is inertially unstable if the absolute vorticity of the basic flow is negative: $f + \zeta < 0$. Note also that large values of PV (e.g., stratospheric) imply a stronger angular momentum gradient, hence resistance to poleward displacement.

b. Equivalent potential vorticity

Let us examine the implications of negative equivalent potential vorticity (EPV) in the Northern Hemisphere:

$$\mathrm{EPV} = \frac{1}{\rho}\frac{\partial \theta_e}{\partial z}(f + \zeta) < 0 \quad , \qquad \text{(3a)}$$

where

$$\theta_e = \theta \; exp\left(\frac{Lw_s}{c_p T}\right) \quad , \qquad \text{(3b)}$$

L = 2.5 x 10^{-6} J kg^{-1} is the latent heat of condensation, w_s is saturation water vapor mixing ratio, C_p = 1005 J kg^{-1} K^{-1} is specific heat at constant pressure, and T is temperature. θ_e allows for energy conservation between vapor phase change and internal energy. According to (3b), in a moist WCB starting at ~12 g/kg in the boundary layer, in the limit of complete elimination of water vapor (a reduction of w_s to 0) , θ would increase by ~32 K (e.g., Holton, 2006). In the UTLS water vapor mixing ratios (~10^{-6}) are reduced by four orders of magnitude relative to a humid boundary layer (~10^{-2}), implying that in the UTLS θ_e is very nearly equal to θ, and that EPV is very nearly equal to PV. Moisture modifies static stability, especially in the boundary layer, therefore the criterion $\partial\theta_e/\partial z < 0$ is the most useful for evaluating static instability.

Eqn. (3) shows that EPV is negative if the atmosphere is either moist statically unstable or if it is inertially unstable. Air that is moist statically unstable that is brought by convection to the base of the stratosphere will be statically stable but it may still have negative EPV, implying that upstream convective instability can lead to downstream inertial instability.

In order to understand the origin of the negative EPV anomalies we consider the PV tendency equation. Due to turbulent mixing and diabatic processes, PV will not be conserved (Andrews et al., 1987). In warm conveyor belts and thunderstorms latent heating dominates.

Following Pomroy and Thorpe (2000), considering the dominant vertical component, and ignoring frictional effects, the PV tendency equation becomes

$$\frac{d\ PV}{dt} = \frac{1}{\rho}\left(\zeta\ \frac{\partial}{\partial z}\left(\frac{d\theta}{dt}\right)\right) \quad . \qquad (4)$$

In the cases to be shown, air found on the equatorward side of the subpolar westerly jet often originates in the moist boundary layer of a subtropical air mass. In considering how this air might be able to facilitate STE, it is important to include water vapor phase changes in defining potential temperature used in calculating PV. Since convective updrafts occur where $\partial\theta_e/\partial z < 0$, it is possible for air with negative EPV to be created and transported into the upper troposphere, as dehydration causes EPV to asymptote to PV, preserving its negative value, with static stability at the base of the stratosphere implying inertial instability. The upward decrease of latent heating in the upper portion of thunderstorms can cause significant negative EPV anomalies.

EPV dynamics are a vital contributor in assessing conditions conducive to conditional symmetric instability (CSI). The concept of EPV has been widely used in studies of CSI in baroclinic systems since CSI was first introduced as a potential mechanism for the generation of frontal rainbands (Bennetts and Hoskins, 1979; Emanuel, 1979; Montgomery and Farrell, 1991; Schumacher and Schultz, 2000; Schultz and Knox, 2007). EPV has proven useful in diagnosing squall lines (Zhang and Cho, 1991), extratropical cyclones (Cao and Cho, 1995; Cao and Zhang, 2004; Brennan et al., 2007), convective snowstorms (Halcomb and Market, 2003), and enhancing our understanding of the dynamics of the UTLS (Hoskins et al., 1985; Morgan, 1998). The present paper focuses on implications of inertial instability for enhancing STE in the UTLS, as highlighted by regions of large negative EPV.

c. Turbulent kinetic energy and Richardson number

Bernard (2013) studied geostrophic turbulence near rapid changes in stratification and found that the forward cascade of buoyancy variance implies an enhanced region of turbulence near the tropopause. Turbulence and gravity waves are noticeably enhanced in the UTLS near westerly jets, and play an important role in mixing (Lindzen and Tung, 1976; Uccellini et al., 1987; Pavelin et al., 2002; Whiteway et al., 2003; Duck and Whiteway, 2005; Koch et al., 2005). Mixing near the jet stream at the tropopause and internal waves breaking in the vicinity of the tropopause are potentially important in the exchange of trace gases such as ozone between the troposphere and the stratosphere (Clayson and Kantha, 2007).

The TKE and Ri patterns to be shown highlight regions of small-scale mixing, which help to exchange air between the stratosphere and troposphere. Kinetic energy per unit mass (TKE, $\varepsilon \sim m^2 \text{ - } s^{-2}$) is a measure of the intensity of turbulence and is defined as

$$\varepsilon = \frac{1}{2}\left(\overline{u'^2} + \overline{v'^2} + \overline{w'^2}\right), \qquad (5)$$

where the overbar indicates time and space averaging of the turbulent eddy variances. The UWNMS contains a prognostic equation for TKE, including advection, buoyancy generation, shear generation, and turbulent dissipation (Tripoli, 1992a, b).

Distributions of the Richardson number, Ri, highlight where convective or shear instability is generating TKE. Ri is the ratio of the mechanical generation of TKE by wind shear to the buoyancy production or inhibition by static stability:

$$\mathrm{Ri} = \frac{\frac{g}{\theta}\frac{\partial\theta}{\partial z}}{\left(\frac{\partial u}{\partial z}\right)^2 + \left(\frac{\partial v}{\partial z}\right)^2}, \qquad (6)$$

where the numerator is equal to the square of the buoyancy frequency. The flow is dynamically unstable for flows with Ri < 0.25 (e.g., Markowski and Richardson, 2010). Once generated, turbulent flow tends to stay turbulent, even for Ri numbers as large as 1.0 (e.g., Stull, 1988).

3. Data and Analysis Methods

During the course of simulating banded precipitation maxima in midlatitude cyclones with the UWNMS, distinctive mesoscale regions of negative EPV were often observed in the UTLS on the equatorward side of the subpolar jet. The spatial and temporal coincidence of pronounced mesoscale stratospheric intrusions on the poleward side of the jet, as seen in PV, θ, and ozone, suggested that perhaps the regions of negative PV were related to the locally enhanced STE. During 6-8 February 2008 (Case 1), phenomena of interest were located over south-central Wisconsin and northern Illinois. During 22-23 April, 2005 (Case 2), negative EPV and local overturning circulations occurred over the Ohio Valley.

Each case is modeled with the UWNMS (Tripoli 1992a, b), initialized with 2.5° European Centre for Medium-range Weather Forecasts (ECMWF) data. Studies of processes in the UTLS, including STE, using the UWNMS include Pokrandt et al. (1996), Hitchman et al. (1999; 2001; 2004), Kittaka et al. (2004), and Büker et al. (2005; 2008). The specified UWNMS resolution for each case is 20 km x 20 km x 300 m, with a grid volume of 152 x 152 x 60 points. The top of the model is set to 16 km, with a 1500 m Rayleigh sponge layer. Each of the simulations was initialized ~24 hours before the phenomena of interest began and continued for 48 hours.

Case 2 was chosen in part because of the availability of high quality globally assimilated ozone fields from GEOS data for 2005 (Stajner, 2008). GEOS ozone data are used to initialize the UWNMS, and to update ozone on the UWNMS side boundaries. Detailed ozone structures evolve in the interior of the UWNMS over the subsequent 48 hours.

Vis5D is used to view the 3D structure of each midlatitude cyclone and the associated dynamical quantities in the UWNMS, and to create trajectories which connect the negative EPV anomalies with upstream convection. National Centers for Environmental Prediction (NCEP) Eta model analyses with 80 km resolution are used to illustrate the synoptic context of the two cases. They provide corroborating evidence of the prevalence of inertial instability on the equatorward side of the subpolar jet.

4. Case Study 1 (6-8 February 2008)

a. Synoptic overview

This destructive mid-winter storm during 6-8 February 2008 featured quasi-stationary snowbands, which trapped over 2000 vehicles for 24 hours on the I-90 freeway in southern Wisconsin, and spawned deadly tornadoes along the cold front throughout the Mississippi and Ohio Valleys. In addition to chronic negative absolute vorticity on the equatorward side of the subpolar jet, convection erupted along the cold front, injecting air into the UTLS between the subtropical and subpolar jets, generating EPV values of less than -3 PVU on the equatorward flank of the subpolar jet.

Figure 1 shows an overview of the synoptic scale features in the lower troposphere associated with the storm at 0000 UT 6 February 2008, using NCEP Eta model reanalyses. Figures 1a and 1b show the surface low pressure centered over southern Missouri and the associated baroclinic zone at 850 hPa. During the low's migration northeastward over Ohio, quasi-stationary snowbands matured and persisted in southwestern Wisconsin and Northern

Illinois, with a characteristic east-west arc-shaped linear configuration, and snowfall in the range 12-18" (exceeding 1" water equivalent in Fig. 1c).

Figure 2 depicts the distribution of PV and wind speed at increasing levels in the UTLS for the same time as in Fig. 1. At 300 hPa a strong subpolar jet with speeds in excess of 70 m/s can be seen in Fig. 2f, arcing from Texas toward the Maritime Provinces, while at 200 and 150 hPa, (Figs. 2d, b), the subtropical jet can be seen extending from Eastern Mexico toward the Mid-Atlantic states. A pronounced southward extension of high polar stratospheric PV air in the 300-250 hPa layer is shown in purple in Fig. 1e, along with a broad anticyclonic arc of negative EPV in dark blue on the equatorward side of the subpolar jet (compare Figs. 2e, f). The pattern of EPV in the 250-200 hPa layer includes negative regions over Illinois and Southern Quebec on the equatorward side of the subpolar jet (compare Figs. 2c, d). The negative PV regions over the Gulf of Mexico and Northern Florida occur on the equatorward side of the subtropical jet and become more extensive in area upon ascending from the 300-250 hPa layer to the 200-150 hPa layer (Figs. 2a, c, e).

A strong spatial correlation exists between the region of negative PV on the equatorward side of the subtropical jet (Figs. 2e, f) and 24-hr accumulated precipitation during 0000 UT 6 February to 0000 UT on 7 February (Fig. 1c), consistent with previous work on symmetric instability and regions of enhanced rainfall.

b. Overview of UWNMS Case 1

Figure 3 shows an oblique view from the southeast of a section from southeastern North Dakota to western Virginia, in the UWNMS simulation at 2230 UT 6 February 2008. The distribution of EPV in the section is shown in panels a, b, and d. Note the regions of negative

EPV in the upper troposphere over Wisconsin and Illinois, adjacent to stratospheric air in the range 1-6 PVU over Minnesota. Figure 3c shows the same EPV contours but also includes a red 60 m/s speed isosurface and blue isosurfaces of negative EPV exceeding -2 PVU, excluding values from behind the section. Note the coincidence of the subpolar jet and region of inertial instability immediately adjacent to the stratospheric air. Note also the separation between the subpolar jet over Iowa and the higher-altitude subtropical jet over Kentucky in this section.

Figure 3b shows the relationship between the EPV distribution, regions of EPV exceeding -2 PVU on the equatorward side of the jet, as well as connections (back trajectory ribbons) to the surface via the WCB and convection along the cold front (4 cm/s green updraft isosurfaces). The regions of strongly negative EPV are seen to originate in the boundary layer over Kansas ~14 hours earlier. A quantitative analysis of EPV evolution along the trajectory is given in the next subsection. The poleward buckling of EPV contours in the UTLS and enhanced signature of a stratospheric intrusion occurs with the arrival of inertially unstable air from convective outflow in the WCB.

The contemporaneous distribution of TKE (blue contours) and Richardson number (black contours) is shown in Fig. 3c. The high vault of negative EPV in the uppermost troposphere generally coincides with low Ri and high TKE, with strong gradients along the base of the stratosphere over the jet core and back into the troposphere along the upper edge of the stratospheric intrusion. Note also the coincidence of TKE exceeding 1.0 $m^2 s^{-2}$ and Ri < 1 in the convective element found in the section over Illinois (Figs. 3b, c).

The evolution of PV and wind fields during the 10 hours preceding Fig. 3 is shown in Fig. 4. At 1300 UT on 6 February 2008 a broad jet with winds exceeding 60 m/s occurred in the UTLS over Iowa (Fig. 4a), with the tropopause sloping gently and monotonically upward toward the south, as indicated by the 1 PVU contour (Fig. 4a) and transition to red (Fig. 4b). At this time there were only modest regions of negative EPV near the jet (Fig. 4a). But by 1830 UT, maximum wind speeds had increased to 75 m/s and shifted poleward, in conjunction with the arrival of convective outflow air with PV < -2 PVU (Figs. 4c, d). By 2100 UT the region of very negative EPV had passed east of the section (Figs. 4e, f). This sequence shows that the tropopause undergoes a distinct folding process, giving the appearance of a poleward and downward circulation of stratospheric air into the troposphere underneath the subpolar jet.

The evolution of the jets, PV, angular momentum, and divergence during 1830 – 2230 UT on 6 February is shown in Fig. 5. At 1830 UT (panel a), high values of angular momentum divided by earth's radius (black contours), are seen to bulge poleward in the UTLS, with the maximum poleward displacement coinciding with the jet maximum (purple contours) and with a region of strong inertial instability (EPV < -2 PVU). The region of actual inertial instability is much larger, as evidenced by the area in which contours of m reverse sign, increasing poleward in the UTLS from Missouri to Minnesota in this section.

The 60 m/s jet isosurface at 2000 UT is highlighted in light blue in Fig. 5b. New regions of strongly negative EPV are approaching the section from the southeast, as old ones recede to the east behind the jet isosurface. Note the large region where $\partial m/\partial y > 0$ in the upper troposphere, tilting poleward with altitude into the jet. The structure of the poleward surge at 2130 UT is seen in Fig. 5c, with the greatest poleward motion occurring in the UTLS, coincident with the greatest poleward excursion of tropical m contours. This poleward surge is a blend of air from the subtropics and from convection along the cold front. This surge extends well into the stratosphere, while an equatorward flow exists in the lower troposphere, with the boundary between the two air masses tilting poleward with height. Differential advection in altitude can readily produce the signature of a stratospheric fold. The poleward convective outflow surge characterized by inertial instability overrides the layer of stratospheric air. This signature of rising warm air and sinking cold air is to be expected for baroclinic synoptic waves. Note also the enhanced region of strong inertial stability, where $-\partial m/\partial y > 0$, at the head of the poleward surge in panels a-c.

The air at the top of the updraft (Fig. 5c) is strongly divergent in the UTLS (dashed contours in Fig. 5d) and is coincident with a region of negative EPV. Theory predicts poleward acceleration, hence horizontal divergence, in a region of inertial instability and initial poleward motion. The striking pattern of divergence and convergence in the troposphere in Fig. 5d is related to inertial instability and the generation of gravity waves, to be discussed below.

An animation of this process is provided in Supplemental movie S1, which highlights the intimate temporal relationship between the arrival of negative EPV anomalies in the UTLS, the poleward surges emanating from the regions of negative EPV, and enhanced signature of a stratospheric intrusion resulting from overriding UTLS air. Figures 3-5 and S1 show that regions of negative EPV within the jet originate in upstream convection and are associated with poleward surges in the westerly jet. This association between negative absolute vorticity and turbulence variables suggests that inertial instability is associated with enhanced mixing of air, as well as with an enhanced intrusion signature. This provides evidence for the hypothesis that strong vertical motion associated with convection creates negative EPV air in the uppermost troposphere, with the resulting inertial instability favoring poleward flow and locally-enhanced stratospheric intrusions.

c. Changes of EPV along the path

Negative anomalies of EPV can form due to diabatic processes associated with surface cooling or with latent heat release in regions of ascent (Morgan, 1997). In convection embedded in the warm upglide sector, a latent heating maximum can generate negative PV through vortex shrinking (Joos and Wernli, 2012). Figures 2a-c show how updrafts transport unstable air from the surface into the the jet, sometimes yielding regions of negative EPV exceeding -3 PVU at heights near 11 km. The negative EPV air found equatorward of the jet initially resided near the surface before being transported to the base of the stratosphere via updrafts exceeding 4 cm/s. These negative EPV anomalies are typically ~1 km thick (3-4 vertical grid points), but the horizontal scale varies considerably: ~40-200 km (2-10 grid points). Back trajectories in Fig. 3 reveal the origin of the negative EPV anomalies as they commenced in the unstable boundary layer and became increasingly more negative while being lifted to the tropopause.

The probe function in Vis5d allows for sampling model variables along the trajectories in this WCB region, including changes of EPV and net diabatic heating along the path. A negative EPV anomaly typically originates near the surface with values around 0 PVU. As the air rises into the upper troposphere, EPV becomes more negative, exceeding -3 PVU on the equatorward side of the subpolar jet. By considering eqns. 3 and 4 one may estimate changes in PV due to the pattern of latent heating. The density factor favors larger EPV anomalies in the upper troposphere. Since latent heating maximizes in the mid-troposphere, then $\frac{\partial}{\partial z}\left(\frac{d\theta}{dt}\right) < 0$ in the upper troposphere, generating negative PV. If a latent heating maximum of 20 K/ 6 hr is assumed near 600 hPa, eqn. (4) suggests that with $\rho \sim 0.3$ kg m^{-3}, f ~ 10^{-4} s^{-1}, and $\delta z \sim 4000$ m, an EPV anomaly of ~ -3 PVU could be generated approaching the 200 hPa level. This calculation supports the mechanism of generating negative EPV described by previous authors.

d. Evolution and comparison of PV, EPV, and absolute vorticity at 8 km

The horizontal signature of RWB in the upper troposphere may be seen in Fig. 4, which quantitatively intercompares PV, EPV, and absolute vorticity at 8 km. The color at left is EPV, while color at right is absolute vorticity, with stratospheric values shown in red and inertially unstable regions in blue. Contours of PV (black) and EPV (white) are also shown in each panel. The evolution of PV over a five hour period is shown, with the upper panels corresponding to 2230 UT 6 February, while the lower panels are for 0330 UT 7 February 2008. A close comparison of the black PV contours and white EPV contours confirms that water vapor in the UTLS makes only a minor quantitative difference between PV and EPV. This is consistent with the reduction of water vapor concentration by four orders of magnitude in going from the surface to the tropopause. The remarkable spatial coincidence of negative regions (blue) of EPV and absolute vorticity shows that in the UTLS, each variable is a reliable indicator of regions of inertial instability, hence may be useful in anticipating mesoscale motions such as radiation of internal gravity waves.

e. A case of "jet suturing" via gravity waves excited by inertial instability?

Figures 7 and 8 show the evolution of the jet pair from the southwest and east, respectively. Supplemental movies S2 and S3 show the evolution of this jet pair for the 48 hour simulation as seen from the west and the east. In this sequence, poleward and upward moving streams of air with EPV < -1 PVU are highlighted in aquamarine, while the 55 m/s speed isosurface is shown in yellow. The right hand panels in Fig. 7 include horizontal sections of absolute vorticity at 5 km. The air masses with large negative EPV are seen to travel upward through an elongated band of negative absolute vorticity at 5 km, connecting to downward-extending fingerlike structures of high wind speed from both jets. This remarkable mesoscale disturbance is related directly to the convection. The fingers of high wind speed appear to have their roots in the region of inertial instability. This mesoscale wave pattern fans out in the vertical, as suggested by the convergence/divergence pattern in Fig. 6d, embracing both jets in the UTLS.

One possible explanation is that the quasi-linear gravity wave-like field perpendicular to the jets is due to inertia-gravity waves generated by the convection and inertial instability, which have a preferred propagation direction antiparallel to the prevailing wind (Dunkerton and Butchart, 1984). Eddy winds associated with gravity waves on the order of 10 m/s would be sufficient to modulate the jet isosurface such as to cause this rib-like structure which connects and modulates the two jets simultaneously, a stitching-together or suturing. This suggests that gravity waves excited by convection and inertial instability may influence the co-evolution of proximal subpolar and subtropical jets.

Figure 8 shows a view from the east of the ascending negative PV streamers merging with downward-extending “stalactites” of high wind speed air. Note the poleward and downward expansion of the jet isosurface from panel a through c. Since the jet core exits the eastern model boundary, one may view snapshots of dollops of air with negative PV as they fly poleward through the subpolar jet, with each event causing a poleward and downward extension of the jet (cf. supplemental movie S3). A salient aspect of supplemental movies S2 and S3 is the appearance of a suturing of the two jets. To the extent that gravity waves break and mix, this may represent a mechanism of interaction between jets generated by convection and inertial instability.

5. Case Study 2 (22 April 2005)

a. Synoptic overview

The spring storm of 22 April 2005 which caused significant precipitation across the Ohio Valley also occurred between subpolar and subtropical jets, ahead of an equatorward-extending stratospheric PV streamer. Even though wind speeds were weaker than in Case 1, EPV still reached values of less than -2 PVU near 13 km. At 1200 UT on 22 April a moderate low pressure system was found over the Ohio Valley, advancing toward the northeast (Fig. 9a). Banded precipitation consistently formed and dissipated on the northwest side of the low pressure center, lingering into the late evening hours of 22 April 2005 (Fig. 9b). A subtropical westerly jet (Fig. 9c) is seen extending from Southern California over Texas and toward the Gulf of Mexico, with notable regions of inertial instability (negative PV in Fig. 9d). Meanwhile, the subpolar westerly jet extended from the Great Lakes toward Eastern Canada, with maximum wind speeds near 50 m/s (Fig. 9d). During the time of the most intense precipitation, a distinct patch of negative EPV (Figs. 9e, f) was found on the anticyclonic shear side of the subpolar jet, consistent with the hypothesis that inertial instability enhances rainfall in midlatitude cyclones. The existence of inertially unstable regions equatorward of westerly jets appears to occur frequently, with convection between two jets particularly conducive for inertial instability-driven poleward acceleration.

b. UWNMS simulation of Case 2 with GEOS ozone

The evolution of EPV (left) and GEOS ozone mixing ratio (right) is shown, together with streamfunction in a meridional section extending from Georgia to southern Ontario, during 1200 - 2230 UT 22 April 2005 (Fig. 10). EPV isosurfaces of -2 PVU are shown in green. High values of PV and ozone are indicated in red. Note the detailed agreement between the patterns of stratospheric PV and stratospheric ozone. The mesoscale details of poleward deformation and stratospheric intrusion are created by the model physics in the UWNMS from coarser initial fields. Inertially unstable regions in the upper troposphere occur immediately above and equatorward of stratospheric intrusions. The association of negative PV anomalies in the upper troposphere and mesoscale disturbances in lower stratospheric PV is notable in panels c-f. The narrow stratospheric intrusion over Indiana shows up clearly in both ozone and PV, coinciding with the arrival of air with substantially negative PV at jet levels. As with Case 1, the merdional streamfunction depicts a deep layer of poleward moving air in the UTLS, which emanates from the convectively and inertially unstable updraft.

The convective updraft over Indiana (green streamfunction) exhibits the canonical signature of positive PV production due to latent heating increasing with height, hence vortex stretching in the lower troposphere, and production of negative PV in the upper troposphere due to vortex compression (Figs. 10a, c, e). The same updraft also brought low values of ozone upward into the UTLS (note the upward extension of light blue in Figs. 10b, d, f).

The development of sharp ozone structures in the UWNMS associated with negative PV regions lends further support to the idea that inertial instability can facilitate stratospheric intrusions. The structure in ozone and PV is consistent with upper tropospheric air surging poleward over stratospheric air, yielding a trailing pattern of “stratospheric intrusion” underneath.

6. Summary of proposed mechanism

Two case studies have been presented which provide evidence for a causal relationship between inertial instability in the UTLS and locally-enhanced STE near midlatitude westerly jets. This phenomenon occurs when a surface low pressure system, with associated convection along a cold frontal boundary, exists between a subtropical and subpolar jet, with WCB updrafts which lift the air to the base of the stratosphere, resulting in areas of enhanced inertial instability near the subpolar jet. It was shown that negative regions of EPV, PV, and absolute vorticity coincide in the UTLS, each serving equally well to indicate inertial instability. This inertial instability facilitates poleward surges of air in the uppermost troposphere, yielding strong shears at the base of the stratosphere, sufficient to give rise to a layer of low Ri and high TKE, which bounds the layer of mixed air that surges poleward over the extratropical troposphere.

A mundane yet perhaps surprising result is that a “stratospheric intrusion” can be created simply by a vertically-limited poleward surge in the UTLS, as shown schematically in Fig. 11. There is no need to stipulate a circulation around a jet to achieve this structure. The poleward expansion of air in the uppermost troposphere over the underlying stratospheric air creates a stratospheric intrusion simply by kinematic folding. In these cases the poleward motion of rising light air advects the subtropical westerly jet northeastward while the equatorward sinking cold air in the lower troposphere tends to cause the subpolar jet to move southeastward. The gravity wave field excited by convective / inertial instability between the two jets modulates the two jets simultaneously, forming a rib-like connection between the two. We find that inertial instability can act to accentuate poleward displacement in the WCB, promoting the large scale baroclinic energy conversion by gravitational adjustment of air with differing density, subject to the ridigity of rotation. The poleward extension of the subtropical westerly jet is resisted by the enhanced meridional gradient of angular momentum (positive PV) of the extratropical lower stratosphere.

Further work is required to diagnose the "suture" signature of jet merger associated with inertial instability in the UTLS. We are currently exploring the seasonality and distribution of inertial instability influences on STE. A companion paper emphasizes the relationship between inertial instability, divergence, poleward surges, and mesoscale jet "flare-ups".

Acknowledgments. We are grateful to the University of Wisconsin Alumni Research Foundation for providing the initial grant for pursuing this idea, and support from NASA grant NNX10AG57G and NSF grant AGS-1256215 which have allowed us to bring these ideas to fruition. We thank Ivanka Stajner for providing the GEOS data for Case 2, Greg Tripoli and Larissa Back for helpful conversations, and Pete Pokrandt and Marek Rogal for their technical expertise.

References

Andrews, D. J., J. R. Holton, and C. B. Leovy, 1987: *Middle Atmosphere Dynamics*, Academic Press, New York, 489 pp.

Bennetts, D. A., and B. J. Hoskins, 1979: Conditional symmetric instability - a possible explanation for frontal rainbands. *Quart. J. Roy. Meteorol. Soc.*, **105**, 945–962.

Bowman, K. P., L. L. Pan, T. Campos, and R. Gao, 2007: Observations of fine-scale transport structure in the upper troposphere from the High performance Instrumented Airborne Platform for Environmental Research. *J. Geophys. Res*., **112**, D18111.

Brennan, M. J., G. M. Lackmann, and K. M. Mahoney, 2007: Potential vorticity (PV) thinking in operations: the utility of nonconservation. *Weather and Forecasting*, **23**, 168-182.

Browell, E. V., E. F. Danielsen, S. Ismail, G. L. Gregory, and S. M. Beck, 1987: Tropopause fold structure determined from airborne lidar in situ measurements. *J. Geophys. Res.*, **92**(D2), 2112–2120.

Browning, K. A., and R. Reynolds, 1994: Diagnostic study of a narrow cold-frontal rainband and severe winds associated with a stratospheric intrusion. *Q. J. Roy. Meteorol. Soc.*, **120**, 235–257.

Büker, M. L., M. H. Hitchman, et al., 2005: Resolution dependence of cross-tropopause ozone transport over East Asia. *J. Geophys. Res*., **110**, D03107.

Büker, M. L., M. H. Hitchman, G. J. Tripoli, R. B. Pierce, E. V. Browell, and J. A. Al-Saadi, 2008: Long-range convective ozone transport during INTEX. *J. Geophys. Res*., **113**, D14S90, doi:10.1029/2007JD009345.

Cao, Z., and H.R. Cho, 1995: Generation of moist potential vorticity in extratropical cyclones. *J. Atmos. Sci.*, **52**, 3263-3281.

Cao, Z., and D.L. Zhang, 2004: Tracking surface cyclones with moist potential vorticity. *Advances in Atmos. Sci.*, **21**, 830-835.

Christenson, C. E., and J. E. Martin, 2014: A synoptic-climatology of Northern Hemisphere polar and subtropical jet superposition events. Submitted to *J. Climate*, **27**.

Clayson, C. A., and L. Kantha, 2008: On turbulence and mixing in the free atmosphere inferred from high-resolution soundings. *J. Atmos. and Oceanic Techn.*, **25**, 833-852.

Cooper, O., et al., 2004: On the life cycle of a stratospheric intrusion and its dispersion into polluted warm conveyor belts. *J. Geophys. Res.*, **109**, D23S09.

Danielsen, E. F., 1968: Stratospheric-tropospheric exchange based on radioactivity, ozone and potential vorticity. *J. Atmos. Sci.*, **25**, 502–518.

Duck, T. J., and J.A. Whiteway, 2005: The spectrum of waves and turbulence at the tropopause. *Geophys. Res. Letts*, **32**, L07801.

Dunkerton, T.J. and N. Butchart, 1984: Propagation and selective transmission of internal gravity waves in a sudden warming. *J. Atmos. Sci.*, **41**, 1443-1460.

Eliassen, A., and E. Kleinschmidt, 1957: Dynamic Meteorology. In *Handbuch der Physik*, 48, Springer-Verlag, 1-154.

Emanuel, K.A., 1979: Inertial instability and mesoscale convective systems. Part I: Linear theory of inertial instability in rotating, viscous fluids. *J. Atmos. Sci.*, **36**, 2425-2449.

Griffiths, M., A. J. Thorpe, and K. A. Browning, 2000: Convective destabilization by a tropopause fold using potential vorticity inversion. *Quart. J. Roy. Meteorol. Soc.*, **126**, 125-144.

Halcomb, C. E., and P. S. Market, 2003: Forcing, instability and equivalent potential vorticity in a Midwest USA convective snowstorm. *Meteorol. Appl.* , **10**, 273-280.

Hayashi, H., M. Shiotani, M., and J. Gille, 2002: Horizontal wind disturbances induced by inertial instability in the equatorial middle atmosphere as seen in rocketsonde observations. *J. Geophys. Res., **107***, 148-227.

Haynes, P. H., C. J. Marks, M. E. McIntyre, T. G. Shepherd, and K. P. Shine, 1991: On the "downward control" of extratropical diabatic circulations by eddy-induced mean zonal forces. *J. Atmos. Sci.*, **48**, 651–78.

Hegglin, M. I., et al., 2008: Validation of ACE-FTS satellite data in the upper troposphere / lower stratosphere (UTLS) using non-coincident measurements. *Atmos. Chem. Phys*., **8**, 1483-1499.

Hitchman, M. H., and C. B. Leovy, 1986: Evolution of the zonal mean state in the equatorial middle atmosphere during October 1978-May 1979. *J. Atmos. Sci.*, **43**, 3159–3176.

Hitchman, M. H., C. B. Leovy, J. C. Gille, P. L. Bailey, 1987: Quasi-stationary zonally asymmetric circulations in the equatorial lower mesosphere. *J. Atmos. Sci.*, **44**, 2219–2236.

Hitchman, M. H., M. L. Büker, and G. J. Tripoli, 1999: Influence of synoptic waves on column ozone during Arctic summer 1997. *J. Geophys. Res*., **104**, 26,547-26,563.

Hitchman, M. H., M. L. Büker, G. J. Tripoli, E. V. Browell, W. B. Grant, T. J. McGee, and J. F. Burris, 2003: Non-orographic generation of arctic PSCs during December 1999. *J. Geophys. Res.*, **108**, SOL 68, 1-16.

Hitchman, M. H., M. L. Büker, G. J. Tripoli, R. B. Pierce, J. A. Al-Saadi, E. V. Browell, M. A. Avery, 2004: A modeling study of an East Asian convective complex during March 2001. *J. Geophys. Res*., **109**, D15S14.

Hitchman, M. H., S. M. Rowe, and G. J. Tripoli , 2014: An inertial view of stratospheric intrusions. To be submitted to *J. Atmos. Sci.*

Hoggatt, B. D., and J. A. Knox, 1998: Non-hydrostatic simulation of unforecast convection in an intense mid-latitude anticyclone. Preprints, *16th Conf. on Weather Analysis and Prediction / 12th Conf. on Numerical Weather Prediction*, Phoenix, AZ Amer. Meteor. Soc., pp. 59-62.

Holton, J. R., P. H. Haynes, M. E. McIntyre, A. R. Douglass, R. B. Rood, and L. Pfister, 1995: Stratosphere-troposphere exchange. *Rev. Geophys*., **33**, 4, 403-439, 95RG02097.

Holton, J. R., 2006: *An Introduction to Dynamic Meteorology.* Academic Press, San Diego, CA, 535 pp.

Homeyer, C. R., K. P. Bowman, L. L. Pan, M. A. Zondlo, and J. F. Bresch (2011), Convective injection into stratospheric intrusions. *J. Geophys. Res*., **116**, D23304.

Hoor, P., H. Fischer, L. Lange, J. Lelieveld, and D. Brunner, 2002: Seasonal variations of a mixing layer in the lowermost stratosphere as identified by the CO-O3 correlation from in situ measurements. *J. Geophys. Res*., **107**(D5), 4044.

Hoskins, B. J., M. E. McIntyre, and A. W. Robertson, 1985: On the use and significance of isentropic potential vorticity maps. *Quart. J. R. Met. Soc*., **111**, 877-946.

Jones, S. C., and A. J. Thorpe, 1992: The three-dimensional nature of 'symmetric' instability. *Quart. J. Roy. Meteorol. Soc.*, **118,** 227-258.

Joos, H. and H. Wernli, 2012: Influence of microphysical processes on the potential vorticity development in a warm conveyor belt - a cast study with the limited area model COSMO. *Q. J. Roy. Meteor. Soc*., **138**, 407-418.

Kittaka, C., et al., 2004: A three-dimensional regional modeling study of the impact of clouds on sulfate distributions during TRACE-P. *J. Geophys. Res.*, **109**, D15S11.

Knippertz, P., and H. Wernli, 2010: A Lagrangian climatology of tropical moisture exports to the Northern Hemispheric Extratropics. *J. Clim*., **23**, 987-1003.

Knox, J. A., 1997: Possible mechanisms of clear-air turbulence in strongly anticyclonic flows. *Mon. Wea. Rev.*, **125**, 1231-1259.

Knox, J. A., 2003: Inertial instability. *Encyclopedia of the Atmospheric Sciences, J. Holton, J. Pyle, and J. Curry, Eds.,* Academic Press, 1004-1013.

Knox, J. A., and V. L. Harvey, 2005: Global climatology of inertial instability and Rossby wave breaking in the stratosphere. *J. Geophys. Res.*, **110**, D06108.

Koch, S.E., Jaminson, B.D., Lu, C., Smith, T.L., Tollerud, E.I., Girz, C., Wang, N., Lane, T.P., Shapiro, M.A., Parrish, D.E., Cooper, O.W., 2005: Turbulence and gravity waves within an upper level front. *J. Atmos. Sci.*, **62**, 3885-3908.

Lang, A. A., and J. E. Martin, 2010: The influence of rotational frontogenesis and its associated shearwise vertical motions on the development of an upper-level front. *Quart. J. Roy. Meteor. Soc.*, **136**, 239-252.

Lang, A., 2011: *The Structure and Evolution of Lower Stratospheric Frontal Zones***.** University of Wisconsin-Madison, Department of Atmospheric and Oceanic Sciences, Madison, WI. Call Number: UW MET Publication No.11.00.L2.

Lindzen, R. S., and K. K. Tung, 1976: Banded convective activity and ducted gravity waves. *Mon. Wea. Rev.*, **104**, 1602-1617.

Madonna, E., H. Wernli, H. Joos, and O. Martius, 2014: Warm conveyor belts in the ERA-Interim data set (1979-2010). Part I: Climatology and potential vorticity evolution. *J. Clim.*, **27**, 3-26.

Manabe, S., and R. T. Wetherald, 1967: Thermal equilibrium of the atmosphere with a given distribution of relative humidity. *J. Atmos. Sci.*, **24** (3), 241-259.

Markowski, P., and Y. Richarsdon, 2010: *Mesoscale Meteorology in Midlatitudes*, John Wiley and Sons, Hoboken, NJ, 407 pp.

Martin, J. E., 2006: The role of shearwise and transverse quasi-geostrophic vertical motions in the mid-latitude cyclone life cycle. *Mon. Wea. Rev.,***134**, 1174-1193.

McIntyre, M. E., and T. N. Palmer, 1983: Breaking planetary waves in the stratosphere. *Nature*, **305**, 593–600.

Mecikalski, J. R., and G. J. Tripoli, 1997: Inertial available kinetic energy and the dynamics of tropical plume formation. *Mon. Wea. Rev*., **126**, 2200–2216.

Montgomery, M. T., and B. F. Farrell, 1991: Moist surface frontogenesis associated with interior potential vorticity anomalies in a semigeostrophic model. *J. Atmos. Sci.*, **48**, 343-367.

Morgan, M. C., 1998: Using piecewise potential vorticity inversion to diagnose frontogenesis. Part I: A partitioning of the Q-Vector applied to diagnosing surface frontogenesis and vertical motion. *Mon. Wea. Rev.*, **127**, 2796-2821.

O'Sullivan, D. J., and M. H. Hitchman, 1992: Inertial instability and Rossby wave breaking in a numerical model. *J. Atmos. Sci.*, **49**, 991-1002.

Pan, L. L., et al., 2007: Chemical behavior of the tropopause observed during the stratosphere-troposphere analyses of regional transport experiment. *J. Geophys. Res.*, **112**, D18110.

Pavelin, E., J. Whiteway, R. Busen, and J. Hacker, 2001: Airbourne observations of turbulence, mixing, and gravity waves in the tropopause region. *J. Geophys. Res.*, **107**, doi:10.1029/2001JD00U77S.

Pokrandt, P. J., G. J. Tripoli, and D. D. Houghton, 1996: Processes leading to the formation of mesoscale waves in the midwest cyclone of 15 December 1987. *Mon. Wea. Rev.*, **124**, 2726– 2752.

Pomroy, H. R., and A. J. Thorpe, 2000: The evolution and dynamical role of reduced upper-tropospheric potential vorticity in Intensive Observing Period One of FASTEX. *Mon. Wea. Rev.*, **128**, 1817-1834.

Randel, W. J., D. J. Seidel, and L. L. Pan, 2007: Observational characteristics of double tropopauses. *J. Geophys. Res.*, **112**, D07309.

Rayleigh, Lord, 1916: On the dynamics of revolving fluids. *Proc. Roy. Soc. London Ser. A*, **92**, 148-154.

Sato, K. and T.J. Dunkerton, 2002: Layered structure associated with low potential vorticity near the tropopause seen in high-resolution radiosondes over Japan. *J. Atmos. Sci.*, **59**, 2782-2800.

Sawyer, J. S., 1949: The significance of dynamic instability in atmospheric motions. *Quart. J. Royal Meteorol. Soc.*, **75**, 364-374.

Schemm, S., H. Wernli, and L. Papritz, 2013: Warm conveyor belts in idealized moist baroclinic wave simulations. *J. Atmos. Sci*., **70**, 627-652.

Schoeffler, F. S., 2013: Large wildfire growth influenced by tropospheric and stratospheric dry slots in the United States. Abstract 5.1, AMS 17th Conference on the Middle Atmosphere, June 2013, Newport, Rhode Island.

Schultz, D. M., and J. A. Knox, 2007: Banded convection caused by frontogenesis in a conditionally, symmetrically, and inertially unstable environment. *Mon. Wea. Rev*., **135**, 2095-2110.

Schumacher, R. S., and D. M. Schultz, 2000: Upper tropospheric inertial instability: Climatologies and possible relationship to severe weather prediction. In *Preprints, 9th Conference on Mesoscale Processes,* Amer. Meteor. Soc., Boston, 372-375.

Schumacher, R. S., D. M. Schultz, and J. A. Knox, 2010: Convective snowbands downstream of the Rocky Mountains in an environment with conditional, dry symmetric, and inertial instabilities. *Mon. Wea. Rev.*, **138**, 4416-4438.

Shapiro, M. A., 1974: A multiple structured frontal zone-jet strea system as revealed by meteorologically instrumented aircraft. *Mon. Wea. Rev.*, **102,** 244-253.

Shapiro, M. A., 1978: Further evidence of the mesoscale and turbulent structure of upper level jet stream-frontal zone systems. *Mon. Wea. Rev.*, **106**, 1100-1111.

Shapiro, M. A., 1980: Turbulent mixing within tropopause folds as a mechanism for the exchange of chemical constituents between the stratosphere and troposphere. *J. Atmos. Sci.* **37,** 994-1004.

Shapiro, M. A., 1981: Frontogenesis and geostrophically forced secondary ciruraltions in the vicinity of jet stream-frontal zone systems. *J. Atmos. Sci.,* **38**, 954-972.

Shapiro, M. A., 1985: Dropwindsonde observations of an Icelandic low and a Greenland mountain lee wave. *Mon. Wea. Rev.*, **113**, 680-683.

Shapiro, M. A., T. Hampel, and A. J. Krueger, 1987: The arctic tropopause fold. *Mon. Wea. Rev*., **115**, 444-454.

Smith, K. S. and E. Bernard, 2013: Geostrophic turbulence near rapid changes in stratification. *Phys. Fluids*., **25**, 046601.

Stajner et al., 2008: Assimilated ozone from EOS-Aura: Evaluation of the tropopause region and tropospheric columns. J. Geophys. Res., 113, D16S32.

Stevens, D. E., and P. E. Ciesielski, 1986: Inertial instability of horizontally sheared flow away from the equator. *J. Atmos. Sci*., **43**, 2845-2856.

Stohl, A., et al. 2003: Stratosphere-Troposphere exchange: A review, and what we have learned from STACCATO. *J. Geophys. Res.*, **108**, 8516.

Stull, R. B., 1988: *An Introduction to Boundary Layer Meteorology*. Springer, 666 pp.

Taylor, G. I, 1923: Stability of a viscous liquid contained between two rotating cylinders. *Phil. Trans. Roy. Soc. London Ser. A*, **223**, 289-343.

Thorncroft, C. D., B. J. Hoskins, and M. E. McIntyre, 1993: Two paradigms of baroclinic wave life cycle behavior. *Quart. J. Roy. Meteor. Soc.*, **119**, 17-55.

Tripoli, G. J., 1992a: An explicit three-dimensional nonhydrostatic numerical simulation of a tropical cyclone, *Meteorol. Atmos. Phys.*, **49**, 229– 254.

Tripoli, G. J., 1992b: A nonhydrostatic numerical model designed to simulate scale interaction. *Mon. Wea. Rev*., **120**, 1342– 1359.

Uccellini, L. W. Koch, E. Steven, 1987: The synoptic and possible energy sources for mesoscale wave disturbances. *Mon. Wea. Rev.*, **115**, 721-729.

Whiteway, J. A., E. G. Pavelin, R. Busen, J. Hacker, and S. Vosper, 2003: Airborne measurements of gravity wave breaking at the tropopause. *Geophys. Res. Letts*., doi:10.1029/2003GL018207.

Wicker, L. J., and W. C. Skamarock, 1998: A time-splitting scheme for the elastic equations incorporating second-order Runge–Kutta time differencing. *Mon . Wea. Rev.*, **126**, 1992-1999.

Zahn, A., C.A.M. Brenninkmeijer, M. Maiss, D.H. Scharffe, P.J. Crutzen, M. Hermann, J. Heintzenberg, A. Wiedersholer, H. Güsten, G. Heinrich, H. Fisher, J.W.M. Cuijpers and P.F.J. van Velthoven, 2000: Identification of extratropical two-way troposphere-stratosphere mixing ased on CARIBIC measurements of O3, CO and ultrafine particles. *J. Geophys. Res*., **105**, 1527-1535.

Zhang, D.-L., H.R. Cho, 1991: The development of negative moist potential vorticity in the stratiform region of a simulated squall line. *Mon. Wea. Rev.*, **120**, 1322-1341.

Zimet, T. K., J. E. Martin, and B. E. Potter, 2007: The influence of an upper-level frontal zone on the Mack Lake wildfire environment. *Meteorol. Appl.*, **14**, 131-147.

Figure Captions

Figure 1. Lower tropospheric synoptic setting for Case 1, as seen in NCEP Eta model reanalyses at 0000 UT 6 February 2008: a) sea level pressure (black contours, interval 4 hPa), b) 850 hPa temperature (color bar, interval 3^{o}C), and c) 24-hr accumulated precipitation during 0000 UT 6 February – 0000 UT 7 February 2008 (color bar, in inches). The location of the surface low pressure center is indicated with an "L".

Figure 2. As in Fig. 1, except for the upper troposphere and lower stratosphere (UTLS) synoptic setting for Case 1, showing layer-averaged PV in the left column (color bar, interval 1 PVU) and wind speed in the right column (color bar, interval 10 m/s) for a) 200-150 hPa PV, b) 150 hPa speed, c) 250-200 hPa PV, d) 200 hPa speed, e) 300-250 hPa PV, and f) 300 hPa speed.

Figure 3. The relationship among convection, inertial instability, jet locations, PV and stratospheric intrusions in UWNMS Case 1 at 2230 UT, 6 February 2008, showing a view from the southwest of a vertical section extending from North Dakota, across the subpolar jet, to the subtropical jet over Kentucky. Panels a), b), and c) show black EPV contours (interval 1 PVU). In panel b) convection along the cold front is indicated with a green (4 cm/s upward motion)

isosurface, the blue (-2 PVU) isosurfaces indicate regions of strong inertial instability in the UTLS, and the ribbons show 22.5-hr back-trajectories from these -2 PVU regions to where they spent the first 10 hours in the unstable boundary layer over Kansas. Panel d) shows the two jets (red 60 m/s isosurface) and the same blue -2 PVU isosurface, but with values behind the section not shown. Panel c) shows the vault of low Ri (black contours, interval 0.5, range 0 - 3), regions of high TKE (blue contours, interval 0.25, range 0 - 1.0), and negative PV in the upper troposphere.

Figure 4. Evolution of PV at 8 km in the UWNMS from 2230 UT 5 February (panels a and b) to 0330 UT 6 February 2008 (panels c and d). In each panel, PV (EPV) contours are shown in black (white), interval 1 PVU. For each time, EPV is shown in color at the left, while absolute vorticity (units 10^{-5} s^{-1}) is shown in color at the right. The color ranges are blue (< 0; inertially unstable), yellow (0 - 1), and red (> 1; stratospheric air).

Figure 5. Meridional sections showing the relationship between absolute angular momentum, wind speed, regions of inertial instability, divergence, and meridional streamfunction, as seen from the west in the UWNMS at 2100 UT on 5 February 2008. Absolute angular momentum per unit mass (divided by earth's radius, green contours with 3-digit labels, every 10 m/s), is shown in panels a), b), and c). Panel a) shows zonal wind speed (black contours with 2-digit labels, every 10 m/s), together with regions of highly inertially unstable regions (EPV < -2 PVU in purple). Panel b) shows the co-location of the poleward-protruding high angular momentum air mass and the 60 m/s wind speed isosurface . Panel c) shows meridional streamfunction in green, indicating the depth of the poleward intrusion. Panel d) shows regions of convergence (solid contours) and divergence (dashed contours), interval 10 x 10^{-5} s^{-1}.

Figure 6. Onset of the effects of inertial instability as seen in vertical sections of PV, wind speed, and regions of inertial instability in the UWNMS for 1300 UT (panels a and b), 1830 UT (panels c and d), and 2100 UT 5 February 2008. PV is shown in the left column in black contours (interval 1 PVU), and in color in the right column (blue < 0; inertially unstable, yellow 0 - 1, red > 1; stratospheric air). Wind speed is contoured (interval 5 m/s) in the right column. A blue isosurface (< -2 PVU) is seen entering the plane of the section from the west in panels c) and d), and exiting behind the plane in panels e) and f).

Figure 7. View from the southwest of the influence of convection, inertial instability, and gravity waves on the subtropical and subpolar jets (55 m/s speed isosurfaces in yellow) in the UWNMS at 2230 UT 5 February (panels a and b), 0330 UT 6 February (panels c and d), and 0600 UT 6 February 2008 (panels e and f). The -1 PVU isosurfaces are shown in light green in each panel. The right hand panels include absolute vorticity (10^{-5} s^{-1}) at 5 km (blue < 0 inertially unstable; yellow 0 – 1, red > 1; stratospheric air).

Figure 8. As in Fig.7 a, c, and e, except view from the east of inertially unstable air causing a poleward surge of the subpolar jet.

Figure 9. Synoptic setting for Case 2, as shown in NCEP Eta model reanalyses at 1200 UT 22 April 2005: a) sea level pressure (black contours, interval 4 hPa), b) 24-hr accumulated precipitation during 0000 UT 22 April – 0000 UT 23 April 2005 (color bar, in inches), c) 200-150 hPa PV (color bar, interval 1 PVU), d) 150 hPa speed, e) 250-200 hPa PV, and f) 300 hPa speed. The location of the surface low pressure center is indicated with an “L”.

Figure 10. Meridional sections in the UWNMS for Case 2 of EPV (color, left column) and ozone mixing ratio (color, right column) as the storm evolved from 1200 UT (a-b), to 2000 UT (c-d), and 2230 UT on 22 April 2005 (e-f). Each panel includes contours of PV (black, interval 1 PVU), meridional streamfunction (green), and -2 PVU isosurfaces (light green). For EPV, blue < -1 PVU, yellow 1-2 PVU, red > 2 PVU. For ozone, dark blue < 50 ppbv, light blue 50-100 ppbv, yellow 100-200 ppbv, red > 200 ppbv.

Figure 11. Schematic diagram of a "stratospheric intrusion" formed by relative motion, in this case a poleward surge of air in the UTLS (time increases downward). Inertial instability aids the poleward intrusion of air into and over the extratropical stratosphere, as the jet strengthens and moves poleward, overriding a thin layer of stratospheric air. Recirculation around the nose of the poleward surge can aid filamentation of the intrusion. Eventually the warm, light and inertially stable lower stratosphere limits further poleward motion.

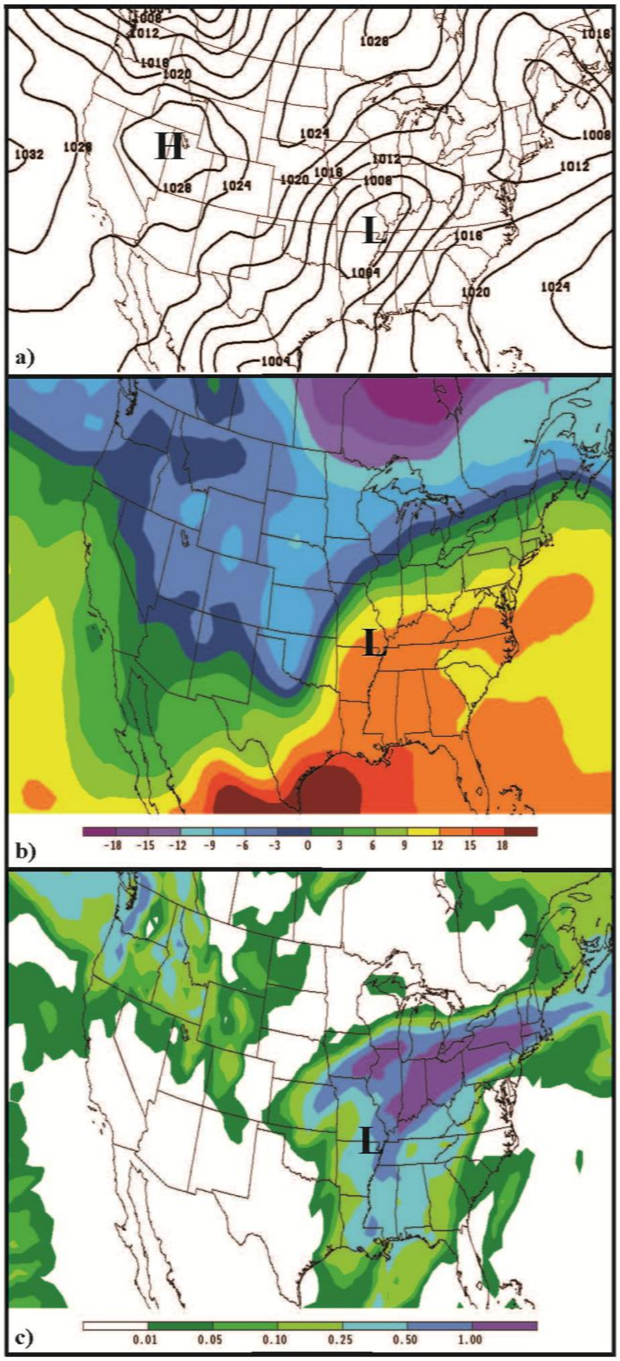

Figure 1. Lower tropospheric synoptic setting for Case 1, as seen in NCEP Eta model reanalyses at 0000 UT 6 February 2008: a) sea level pressure (black contours, interval 4 hPa), b) 850 hPa temperature (color bar, interval 3°C), and c) 24-hr accumulated precipitation during 0000 UT 6 February – 0000 UT 7 February 2008 (color bar, in inches). The location of the surface low pressure center is indicated with an "L".

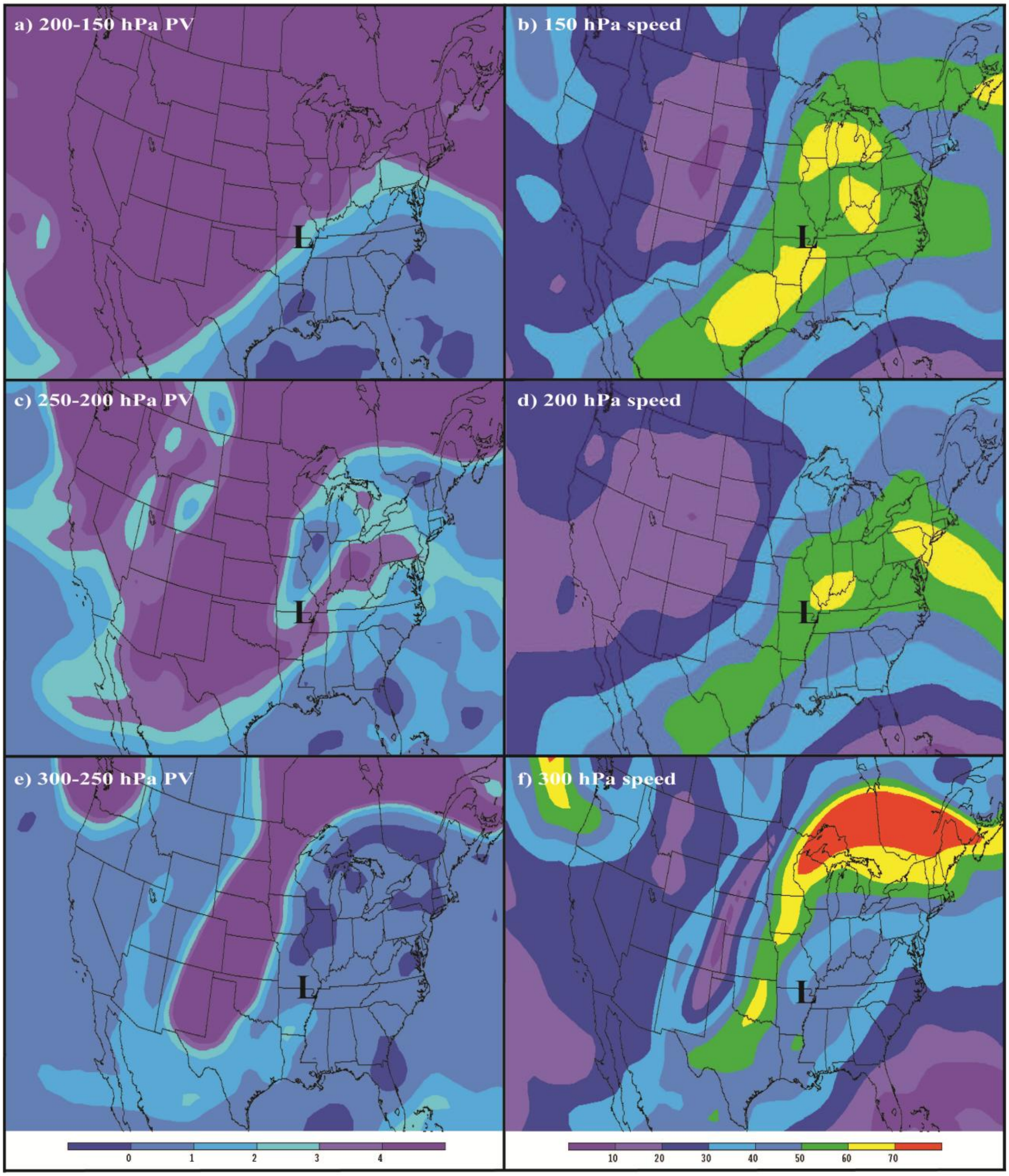

Figure 2. As in Fig. 1, except for the upper troposphere and lower stratosphere (UTLS) synoptic setting for Case 1, showing layer-averaged PV in the left column (color bar, interval 1 PVU) and wind speed in the right column (color bar, interval 10 m/s) for a) 200-150 hPa PV, b) 150 hPa speed, c) 250-200 hPa PV, d) 200 hPa speed, e) 300-250 hPa PV, and f) 300 hPa speed.

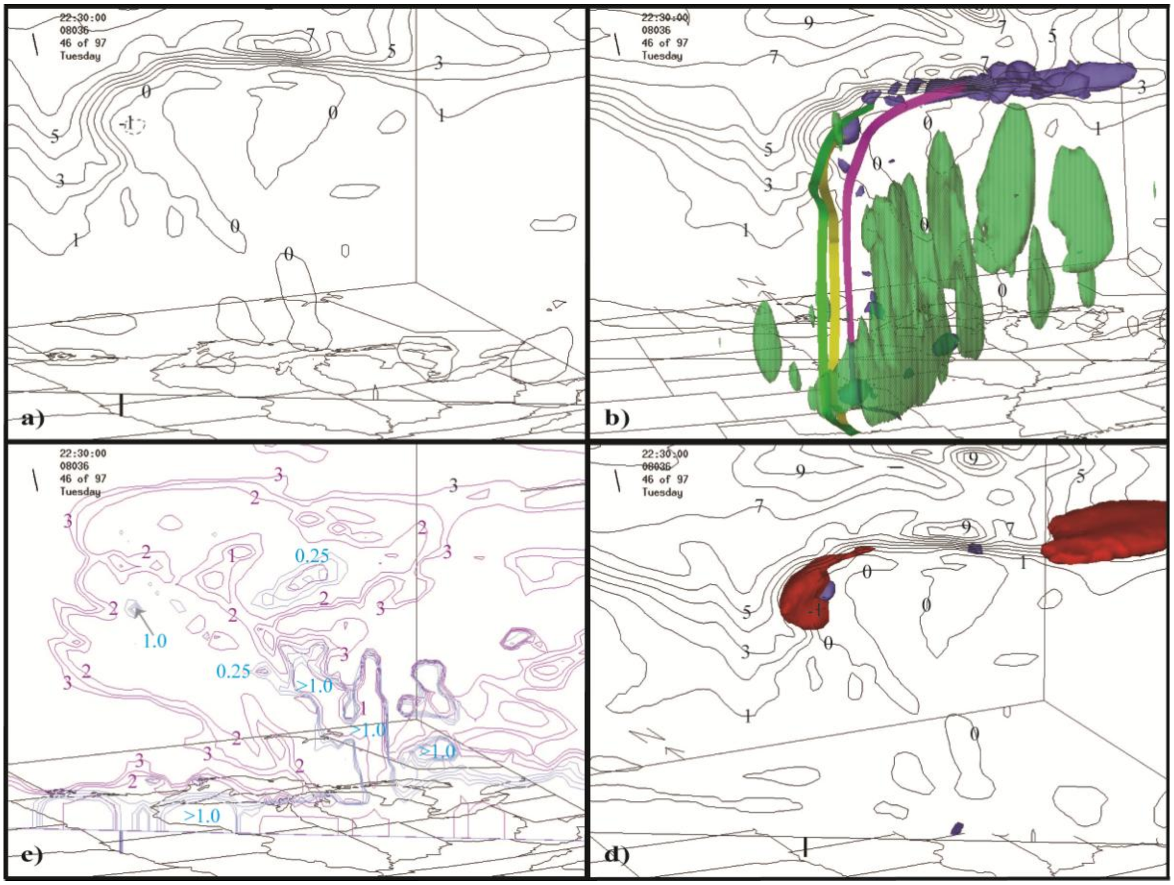

Figure 3. The relationship among convection, inertial instability, jet locations, PV and stratospheric intrusions in UWNMS Case 1 at 2230 UT, 6 February 2008, showing a view from the southwest of a vertical section extending from North Dakota, across the subpolar jet, to the subtropical jet over Kentucky. Panels a), b), and c) show black EPV contours (interval 1 PVU). In panel b) convection along the cold front is indicated with a green (4 cm/s upward motion) isosurface, the blue (-2 PVU) isosurfaces indicate regions of strong inertial instability in the UTLS, and the ribbons show 22.5-hr back-trajectories from these -2 PVU regions to where they spent the first 10 hours in the unstable boundary layer over Kansas. Panel d) shows the two jets (red 60 m/s isosurface) and the same blue -2 PVU isosurface, but with values behind the section not shown. Panel c) shows the vault of low Ri (black contours, interval 0.5, range 0 - 3), and regions of high TKE (blue contours, interval 0.25, range 0 - 1.0).

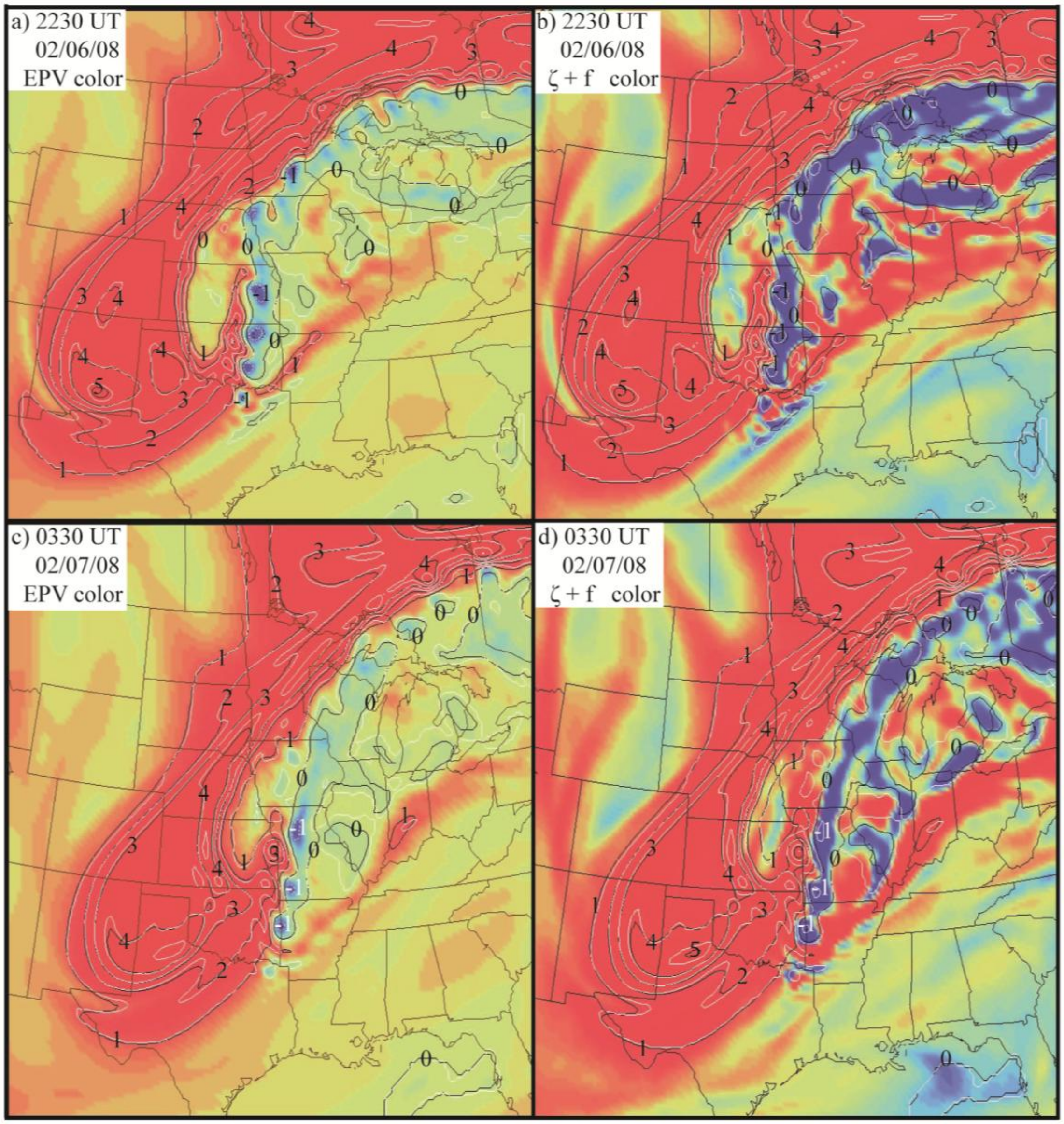

Figure 4. Evolution of PV at 8 km in the UWNMS from 2230 UT 5 February (panels a and b) to 0330 UT 6 February 2008 (panels c and d). In each panel, PV (EPV) contours are shown in black (white), interval 1 PVU. For each time, EPV is shown in color at the left, while absolute vorticity (units 10^{-5} s^{-1}) is shown in color at the right. The color ranges are blue (< 0; inertially unstable), yellow (0 - 1), and red (> 1; stratospheric air).

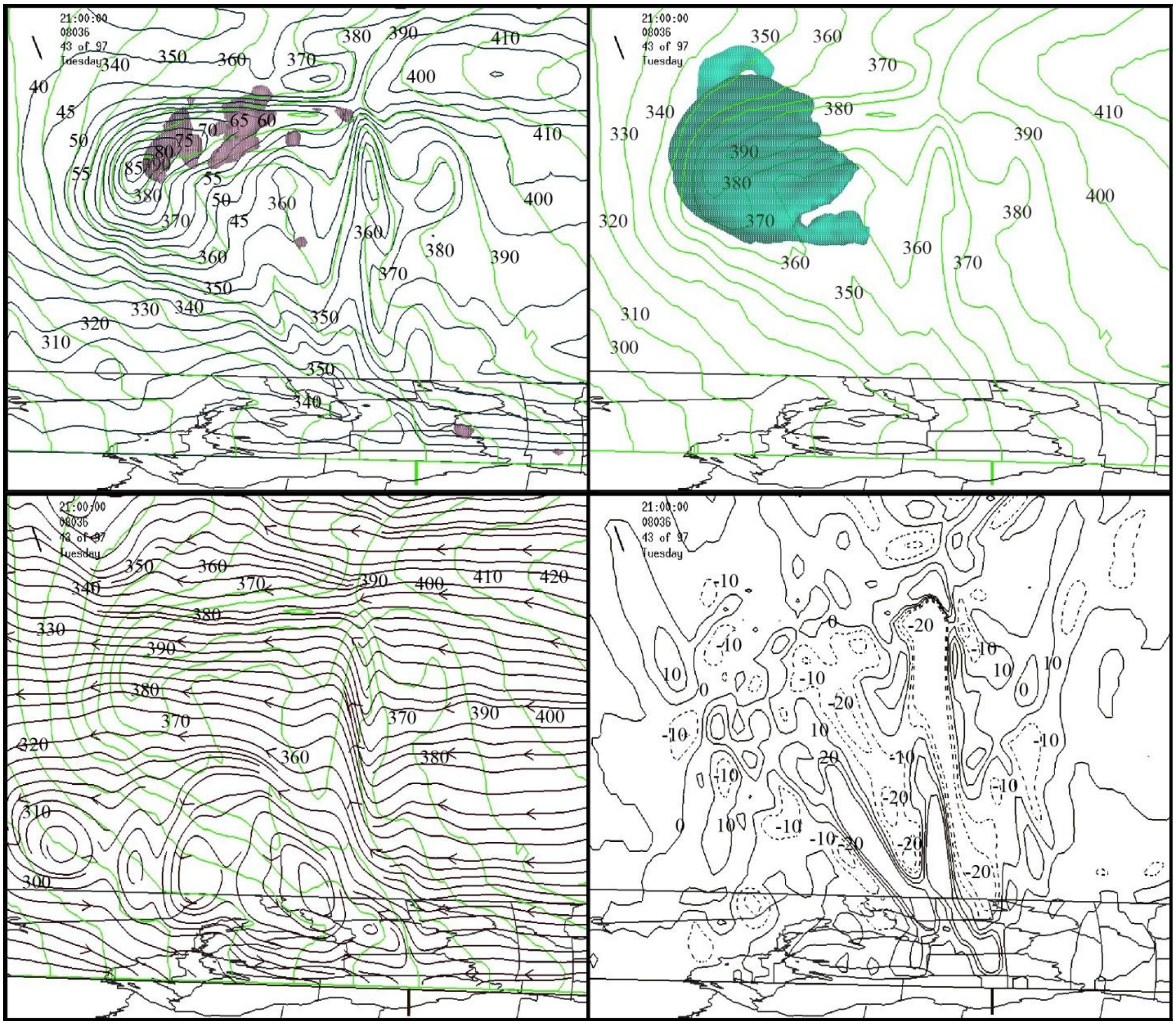

Figure 5. Meridional sections showing the relationship between absolute angular momentum, wind speed, regions of inertial instability, divergence, and meridional streamfunction, as seen from the west in the UWNMS at 2100 UT on 5 February 2008. Absolute angular momentum per unit mass (divided by earth's radius, green contours with 3-digit labels, every 10 m/s), is shown in panels a), b), and c). Panel a) shows zonal wind speed (black contours with 2-digit labels, every 10 m/s), together with regions of highly inertially unstable regions (EPV < -2 PVU in purple). Panel b) shows the co-location of the poleward-protruding high angular momentum air mass and the 60 m/s wind speed isosurface . Panel c) shows meridional streamfunction in green, indicating the depth of the poleward intrusion. Panel d) shows regions of convergence (solid contours) and divergence (dashed contours), interval 10 x 10^{-5} s^{-1}.

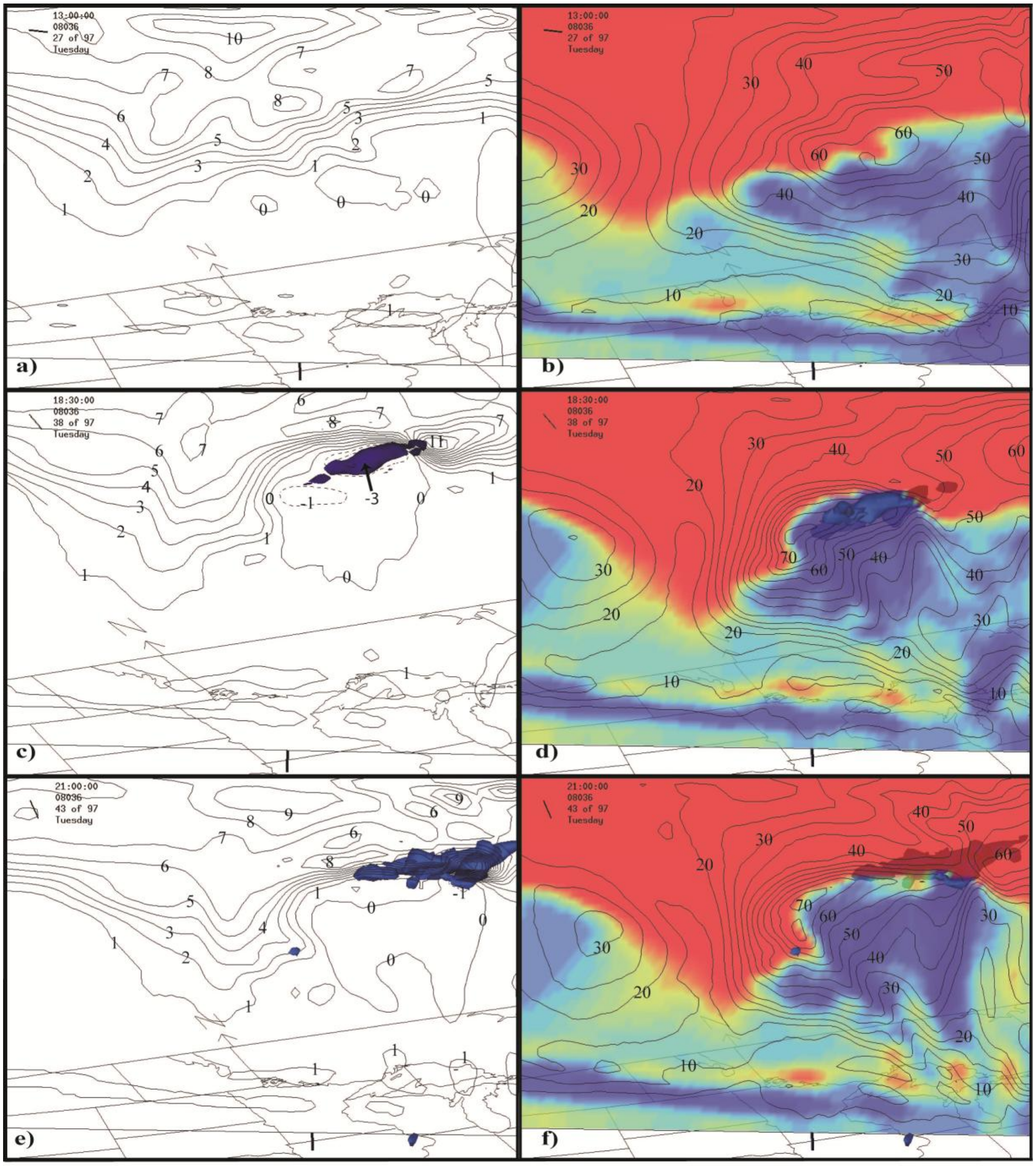

Figure 6. Onset of the effects of inertial instability as seen in vertical sections of PV, wind speed, and regions of inertial instability in the UWNMS for 1300 UT (panels a and b), 1830 UT (panels c and d), and 2100 UT 5 February 2008. PV is shown in the left column in black contours (interval 1 PVU), and in color in the right column (blue < 0; inertially unstable, yellow 0 - 1, red > 1; stratospheric air). Wind speed is contoured (interval 5 m/s) in the right column. A blue isosurface (< -2 PVU) is seen entering the plane of the section from the west in panels c) and d), and exiting behind the plane in panels e) and f).

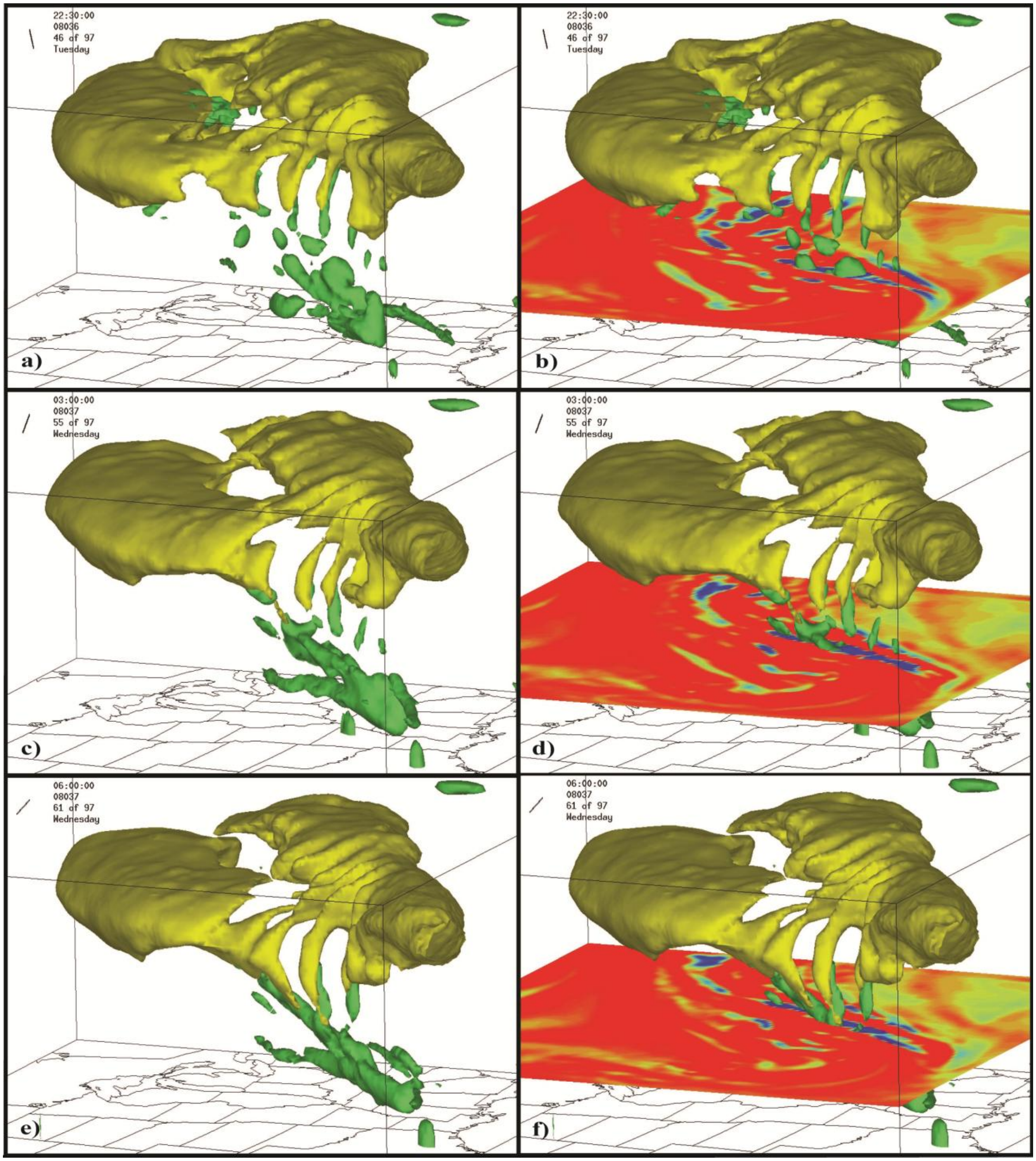

Figure 7. View from the southwest of the influence of convection, inertial instability, and gravity waves on the subtropical and subpolar jets (55 m/s speed isosurfaces in yellow) in the UWNMS at 2230 UT 5 February (panels a and b), 0330 UT 6 February (panels c and d), and 0600 UT 6 February 2008 (panels e and f). The -1 PVU isosurfaces are shown in light green in each panel. The right hand panels include absolute vorticity (10^{-5} s^{-1}) at 5 km (blue < 0 inertially unstable; yellow 0 – 1, red > 1; stratospheric air).

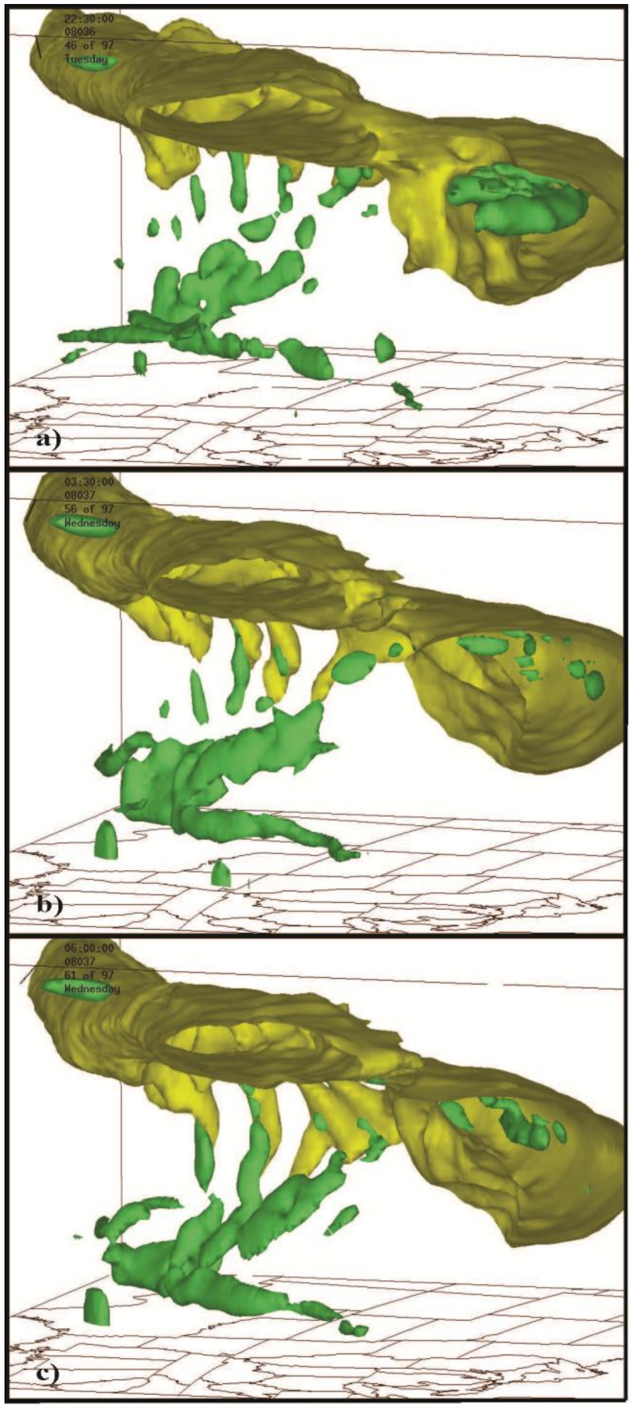

Figure 8. As in Fig.7 a, c, and e, except view from the east of inertially unstable air causing a poleward surge of the subpolar jet.

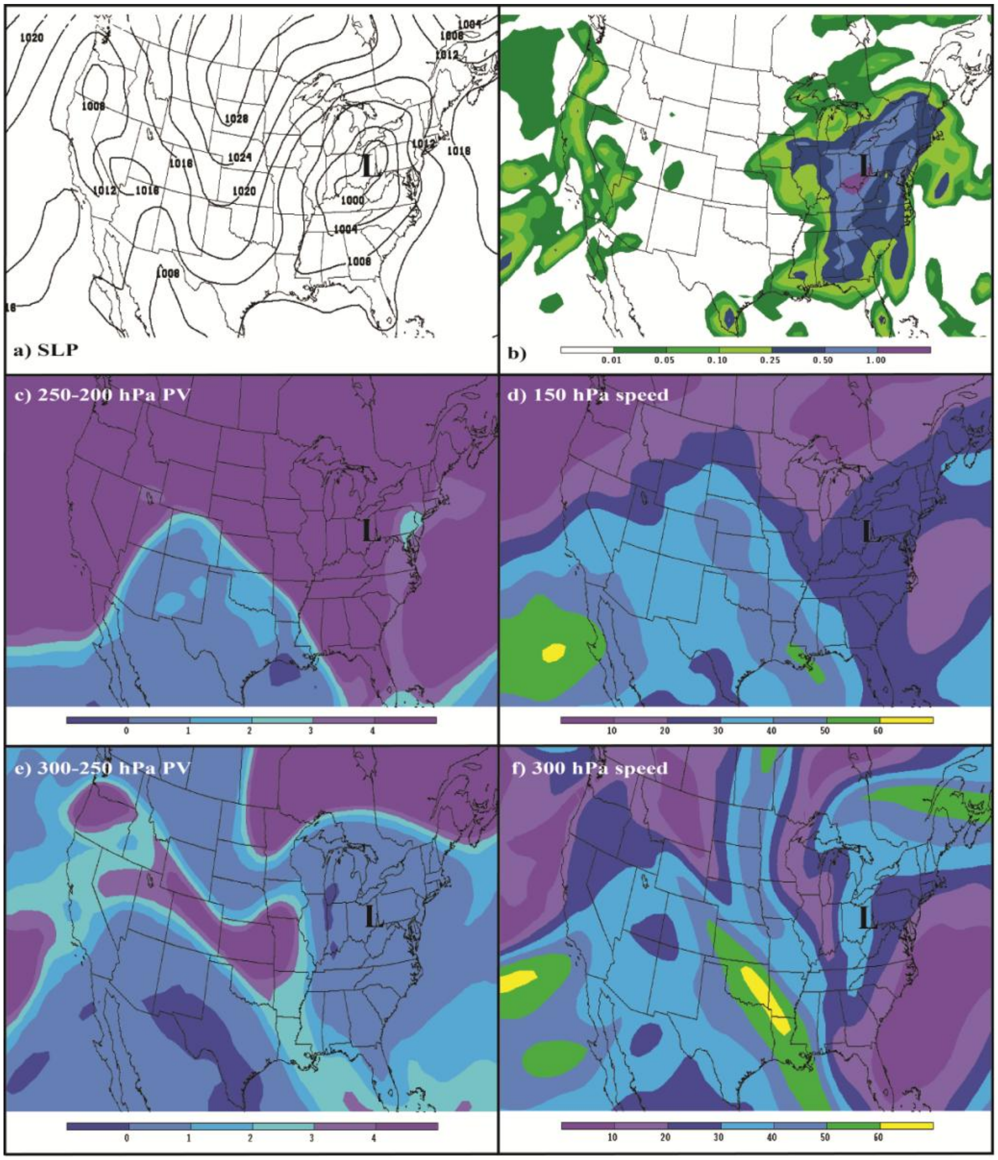

Figure 9. Synoptic setting for Case 2, as shown in NCEP Eta model reanalyses at 1200 UT 22 April 2005: a) sea level pressure (black contours, interval 4 hPa), b) 24-hr accumulated precipitation during 0000 UT 22 April – 0000 UT 23 April 2005 (color bar, in inches), c) 200-150 hPa PV (color bar, interval 1 PVU), d) 150 hPa speed, e) 250-200 hPa PV, and f) 300 hPa speed. The location of the surface low pressure center is indicated with an “L”.

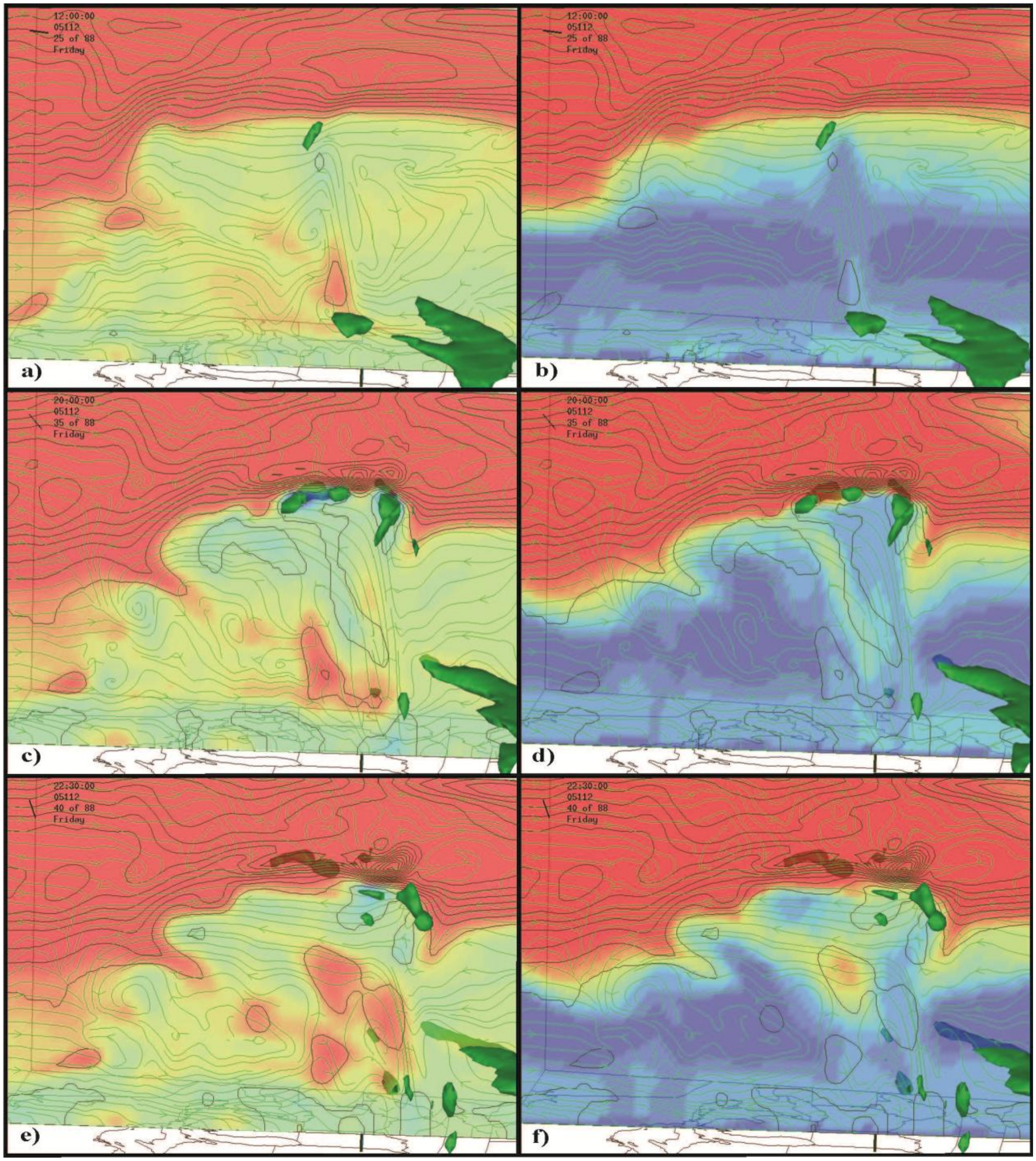

Figure 10. Meridional sections in the UWNMS for Case 2 of EPV (color, left column) and ozone mixing ratio (color, right column) as the storm evolved from 1200 UT (a-b), to 2000 UT (c-d), and 2230 UT on 22 April 2005 (e-f). Each panel includes contours of PV (black, interval 1 PVU), meridional streamfunction (green), and -2 PVU isosurfaces (light green). For EPV, blue < -1 PVU, yellow 1-2 PVU, red > 2 PVU. For ozone, dark blue < 50 ppbv, light blue 50-100 ppbv, yellow 100-200 ppbv, red > 200 ppbv.

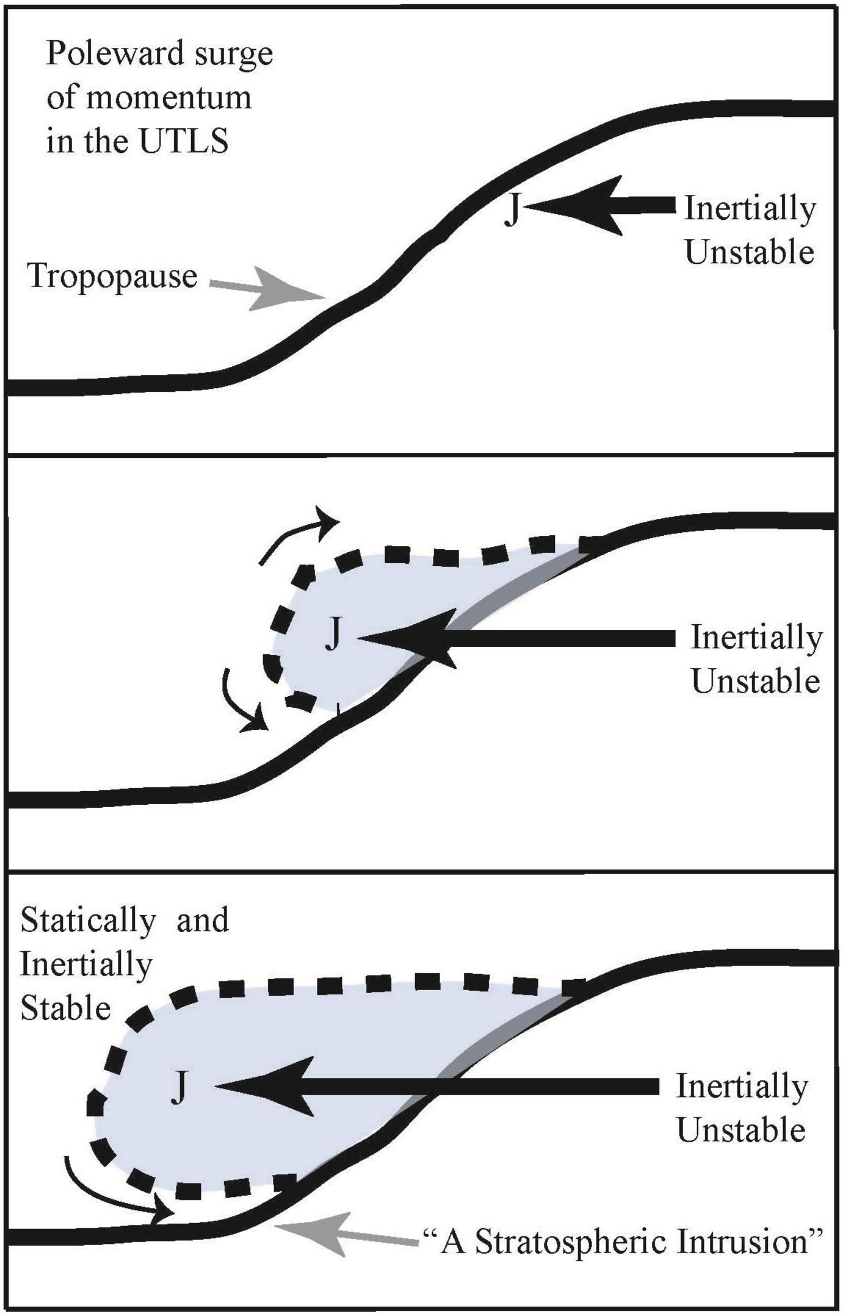

Figure 11. Schematic diagram of a "stratospheric intrusion" formed by relative motion, in this case a poleward surge of air in the UTLS (time increases downward). Inertial instability aids the poleward intrusion of air into and over the extratropical stratosphere, as the jet strengthens and moves poleward, overriding a thin layer of stratospheric air. Recirculation around the nose of the poleward surge can aid filamentation of the intrusion. Eventually the warm, light and inertially stable lower stratosphere limits further poleward motion.